NASA CR-134986

A THEORETICAL EVALUATION OF RIGID BAFFLES IN SUPPRESSION OF COMBUSTION INSTABILITY

by

M. R. Baer and C. E. Mitchell

COLORADO STATE UNIVERSITY

prepared for

NATIONAL AERONAUTICS AND SPACE ADMINISTRATION

NASA Lewis Research Center
Grant NGR 06-002-095
Richard J. Priem, Project Manager

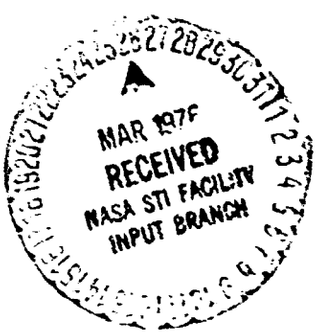

NASA CR-134986

A THEORETICAL EVALUATION OF RIGID BAFFLES IN SUPPRESSION OF COMBUSTION INSTABILITY

by

M. R. Baer and C. E. Mitchell

COLORADO STATE UNIVERSITY

prepared for

NATIONAL AERONAUTICS AND SPACE ADMINISTRATION

NASA Lewis Research Center
Grant NGR 06-002-095

Richard J. Priem, Project Manager

1. Report No. NASA CR 134986	2. Government Accession No.	3. Recipient's Catalog No.
4. Title and Subtitle A Theoretical Evaluation of Rigid Baffles in Supression of Combustion Instability		5. Report Date March 1976 6. Performing Organization Code
7. Author(s) M. R. Baer, C. E. Mitchell		8. Performing Organization Report No. 10. Work Unit No.
9. Performing Organization Name and Address Colorado State University Fort Collins, Colorado 80523		11. Contract or Grant No. NGR 06-002-095 13. Type of Report and Period Covered
12. Sponsoring Agency Name and Address National Aeronautics and Space Administration Washington, D.C. 20546		14. Sponsoring Agency Code

15. Supplementary Notes
Project Manager, Richard J. Priem, Chemical Propulsion Division, NASA Lewis Research Center, Cleveland, Ohio

16. Abstract

An analytical technique for the prediction of the effects of rigid baffles on the stability of liquid propellant combustors is presented. This analysis employs both two and three dimensional combustor models characterized by concentrated combustion sources at the chamber injector and a constant Mach number nozzle. An eigenfunction-matching method is used to solve the linearized partial differential equations describing the unsteady flow field for both models. Boundary layer corrections to this unsteady flow are used in a mechanical energy dissipation model to evaluate viscous and turbulence effects within the flow. An integral instability relationship is then employed to predict the decay rate of the oscillations.

Results of this analysis agree qualitatively with experimental observations and show that sufficient dissipation exists to indicate that the proper mechanism of baffle damping is a fluid dynamic loss. The response of the dissipation model to varying baffle blade length, mean flow Mach number, oscillation amplitude, baffle configuration and oscillation mode is examined.

17. Key Words (Suggested by Author(s))	18. Distribution Statement		
Combustion Instability Injector face baffles Liquid rockets	Unclassified - unlimited		
19. Security Classif. (of this report) Unclassified	20. Security Classif. (of this page) Unclassified	21. No. of Pages 137	22. Price* $3.00

*For sale by the National Technical Information Service, Springfield, Virginia 22151

Foreword

The research reported here was conducted at Colorado State University during the period December 1, 1973 to December 31, 1975 and was supported by NASA Grant NGR 06-002-095. The work was done under the management of the NASA Technical Monitor, Dr. Richard J. Priem, Chemical Rockets Division, NASA Lewis Research Center.

ABSTRACT

An analytical technique for the prediction of the effects of rigid baffles on the stability of liquid propellant combustors is presented. This analysis employs both two and three dimensional combuster models characterized by concentrated combustion sources at the chamber injector and a constant Mach number nozzle. An eigenfunction-matching method is used to solve the linearized partial differential equations describing the unsteady flow field for both models. Boundary layer corrections to this unsteady flow are used in a mechanical energy dissipation model to evaluate viscous and turbulence effects within the flow. An integral stability relationship is then employed to predict the decay rate of the oscillations.

Results of this analysis agree qualitatively with experimental observations and show that sufficient dissipation exists to indicate that the proper mechanism of baffle damping is a fluid dynamic loss. The response of the dissipation model to varying baffle blade length, mean flow Mach number, oscillation amplitude, baffle configuration and oscillation mode is examined.

TABLE OF CONTENTS

LIST OF FIGURES

NOMENCLATURE

a	speed of sound
A_m^μ or $A_{\ell m}^\mu$	coefficient matrix for velocity potential in baffle compartments
B_m or $B_{\ell m}$	coefficient matrix for velocity potential in main chamber
E_{dis}	mechanical energy dissipation due to viscous effects
E_{dis}^T	mechanical energy dissipation due to turbulence effects
$\vec{e}_k$	axial unit vector
i	unit complex $\sqrt{-1}$
$J_m(\ )$	Bessel function of 1st kind of order m
$\hat{\ell}$	radial mode integer
ℓ	integer
L	chamber characteristic length
m	integer
$\hat{m}$	Transverse mode integer
$\dot{m}$	mass flow rate
M	steady state Mach number
n	interaction index

N	total number of baffle cavities
P	pressure
$\vec{q}$	velocity
r	radial coordinate
R	chamber radius
S_B	baffle blade surface
S_{inj}	injector surface
S_{noz}	nozzle entrance surface
T	temperature or baffle blade thickness
t	time
u	axial velocity
y	transverse coordinate
z	axial coordinate
z_B	baffle blade length
α	circumferential coordinate at baffle blade tip
γ	ratio of specific heats
ϵ	wave amplitude
η	coordinate normal to surface covered by boundary layer

ϑ circumferential coordinate

λ decay rate

$\lambda^B_{\ell m}$ ℓ^{th} root of $\frac{d}{dr} J_{\frac{mN}{2}} (\lambda^B_{\ell m} r) = 0$

$\lambda^C_{\ell m}$ ℓ^{th} root of $\frac{d}{dr} J_{\pi} (\lambda^C_{\ell m} r) = 0$

μ integer specifing a particular baffle compartment

μ_ν molecular viscosity

μ_{eff} turbulent effective viscosity

ρ density

$\bar{\tau}$ sensitive time lag

ϕ velocity potential

Ψ streamfunction

ω complex frequency

ω_r real part of complex frequency

ζ radial coordinate near baffle blade tips

δ boundary layer thickness

$\delta_{m,\hat{m}}$ Kronecker delta

Subscripts:

B	baffle quantity
C	main chamber quantity
r	real part

Superscripts:

B	baffle quantity
C	main chamber quantity
~	steady state quantity
*	dimensional quantity
^	designates a particular mode of oscillation
'	perturbation quantity

Mathematical symbols:

$\overline{\quad}$	complex conjugate
$\langle\ \rangle$	time average
$O(\ )$	order
$\frac{D(\ )}{Dt}$	total derivative = $\frac{\partial}{\partial t} + \vec{q}\cdot\vec{\nabla}$

Section I

INTRODUCTION

A complex sequence of chemical and physical processes takes place during combustion and under certain conditions can couple with the associated fluid dynamics to produce oscillations in the thermodynamic variables and velocity flow field. Random, small amplitude fluctuations characterized by the presence of turbulence are typical of this flow. A distinct oscillatory behavior, in addition to the turbulence, may also be present. These oscillations are organized with a distinct frequency and can possess an amplitude which grows with time. This type of unsteady behavior is termed combustion instability.

High frequency instability or resonant combustion produces several detrimental effects and is of major concern in liquid propellant rocket combustion chamber design. These instabilities have frequencies typically between 1000 to 15,000 hertz and have been measured at amplitudes between 10 to 1,000 percent of steady state values. Wall compatability poses a problem with the occurence of this phenomena due to increased stress and heat transfer rates. These effects can then lead to rupture and thermal failure of the chamber walls. Other secondary problems arise from destruction of controls and safety devices placed internally within the chamber, decreased performance, uncontrolled impulse and variation in thrust vector.

As engine development has progressed, combustor designs have required increased performance characteristics and have utilized more energetic propellants with injectors designed to promote more efficient combustion. These influences tend to encourage the occurrence of

combustion instability. Instead of altering these combustion characteristics, mechanical damping devices have been used to improve stability. Two such devices have been successfully used to suppress instability.

One of these devices is the acoustic liner. It is a series of Helmholtz resonators or circumferential slots that are placed or machined on the periphery of the chamber. Jet losses are responsible for the damping that is produced by these devices. Experimental verification of this mechanism has been established[1] and a strong theoretical basis for design of these devices has been established in several combustion instability analyses.[2,3] However, designers are reluctant to use this mechanical damping device because it creates local hot spots on the chamber walls and heat transfer becomes an important consideration.

The other device that is used is termed a baffle. It is a series of blades attached to the injector surface protruding axially down the chamber. This device was first proposed in 1954[4] and was for some time regarded as the panacea to the combustion instability problem. Sufficient experimental verification of the stability improvement of combustors with baffles has been produced, however total reliability of this device has been limited since a few combustors have failed to gain stability improvement with the addition of a baffle. A theoretical treatment of baffle damping is needed to avoid these anomalies and aid in design. Unfortunately, no satisfactory theory exists and design of the baffle has remained a black art which utilizes several empirical rules that may or may not be applied effectively in a particular engine configuration.

Several baffle configurations have been conceived by designers (refer to Figure 1) particularly with respect to blade arrangement and blade shape. However, utilizing these designs requires expensive and time consuming full scale tests. Heat transfer aspects of these devices are also of importance but because the baffle is an internal device separable from the combustor walls these considerations aren't critical as far as the structural integrity of the chamber is concerned.

Before discussing the theoretical attempts to model the problem, the relevant experimental observations will be examined. First, it is observed that stability is likely to improve with the addition of the baffle. Furthermore, an increase in blade length generally increases the stability of the chamber. Care with respect to this rule must be taken since a baffle can be too short or too long.[5] Figure 2 depicts experimental measurements of decay rate for various baffle blade lengths.[6] This decay rate is representative of the oscillations within a baffled combustor experiencing flow or combustion conditions that would produce neutrally stable oscillations in the chamber without baffles. Two separate flows, cold flow (flow without combustion or mean flow) and hot flow conditions are examined in Figure 2 and show similar stability behavior.

Secondly, it is observed that the addition of a baffle to a chamber depresses the preferred frequencies of the oscillations within the chamber. The frequency becomes even smaller with an increase in blade length (refer to Figure 3). In conjunction with these results it is noted that baffle configuration has a minor influence in the problem, (several baffle configurations are depicted in Figures 2 and 3), providing that the configuration does not coincide with the tangential

velocity nodes downstream of the baffle. For example, an evenly spaced three bladed baffle has little influence on damping a third transverse mode oscillation because the velocity nodal lines (in the circumferential direction) are coincident with the baffle blades and the resulting wave description within the baffle compartments and main chamber are identical.

Cold flow acoustic tests conducted at NASA Lewis by Wieber[7] have produced further information about baffle damping. Test chambers constructed without combustion and nozzle influences indicate the damping mechanism is a fluid dynamic loss which can be independent of combustion and nozzle effects. This result is also displayed in the similar stability trends in the cold flow tests and hot firing tests given in Figures 2 and 3. From this study it is also concluded that the increase in surface area and the associated viscous loss (as predicted by an idealized theory)[8] is insufficient to account for the energy loss. In fact, decay rate measurements are an order of magnitude larger than predicted by theory.

A comprehensive theoretical treatment of baffle damping has been fruitless in previous investigations. Several analytical models have failed because of oversimplification of the problem. One such study performed by Reardon[9] simplifies the geometry of the problem and requires only one dimensional oscillations in the baffle cavities which interact with three dimensional oscillations downstream of the baffle. The influences of combustion, nozzle and mean flow effects are treated and a decay rate calculation is made. Frequency prediction with this model is in agreement with experimental observation, however, results from this study indicate a mechanism for the baffle damping that is

totally dependent upon another loss producing device (i.e. a nozzle) in the system. This conclusion doesn't account for damping in the pure acoustic flow situation which has been observed in Wieber's work mentioned earlier. Also the stability predictions are underestimated and do not show the proper trends.

A second model that was considered for analytic treatment has been suggested by Sirignano and Strahle.[10] This model employs a distorted injector surface (resembling a particular baffle configuration) and treats a surface perturbation problem. The equation governing the resulting flow field are given and an asymptotic representation of the solution is obtained. However, since no energy loss or gain considerations are made, stability prediction with this solution is futile.

The final analysis to be discussed is a model devised by Oberg, et. al.[11] This study treats three dimensional oscillations everywhere in the baffled chamber. An inviscid flow with the influences of concentrated combustion, nozzle and mean flow is studied using a variational Green's function method. Separate solutions are expanded within the baffle compartments and matched with the solution downstream of the baffle. Pressure and axial velocity are approximately matched at the interface connecting these regions and produce the complete solution. Owing to the variational method, these matching conditions are approximated and in certain cases are grossly represented. However, frequency trends are properly predicted and the acoustic flow field is in agreement with experimental observation. This solution also predicts a strong flow around the baffle tips which is in agreement with experimental observation. The major failure of this theory is its improper stability prediction of baffled chambers. The solution predicts a

pressure rise at the injector end of the chamber and a pressure loss at the nozzle. Using the Rayleigh criterion[12] (see also Chapter V) a destabilizing influence for the baffles is then indicated. In other words, more energy can be added at the injector and the nozzle extracts less energy which results in an unstable flow.

In reviewing the forementioned theories, it is apparent that wave alteration is not the mechanism of baffle damping, failing as indicated by the Rayleigh criterion. A second damping mechanism has also been considered and is a change in combustion characteristics. However, Wieber's experimental evidence indicates this cannot be the only mechanism. Concentrating the combustion at the injector overemphasizes the energy input in the flow. An investigation of distributing the combustion shows that it is insufficient to relax the combustion energy input and baffles still cause an overall destabilizing influence.

A third possible mechanism is suggested from Oberg's work and Wieber's experimental results. Since a strong flow near the baffle blade tips is indicated in Oberg's solution, viscous and turbulence losses may produce sufficient energy dissipation to overcome the driving effect of wave alteration. This fluid dynamic loss is unaccounted for in Wieber's attempt to explain his experimental results, since it occurs locally at the tips of the baffle blades and departs from idealized theory. In fact, this dissipation mechanism has been neglected in all previous theories.

The inclusion and estimation of this fluid dynamic loss is the purpose of this analysis. An eigenfunction-matching method, which parallels Oberg's solution is used to represent the unsteady core flow. An exact match, in contrast to Oberg's variational approximation,

produces the desired solution. Boundary layer corrections in the baffle tip region are added to the solution and applied to a mechanical energy dissipation model. Results from this study show the importance of this energy loss mechanism.

Section II

THEORY--TWO DIMENSIONAL CHAMBER SOLUTION

Owing to the mathematical complexity of this problem, a simplification of combustor geometry to a two dimensional rectangular chamber is made. This choice of geometry is used purely as a diagnostic tool for the more realistic three dimensional flow, and as such predicts gross stability trends. However, this model clearly shows the mathematical foundations of the problem of interest and application to the three dimensional chamber is merely a mathematical extension. This analysis follows in the next chapter.

The baffles enter the problem as discontinuities which rigidly protrude axially downstream of the injector end of the chamber. The chamber is then split into multiple evenly spaced rectangular compartments which are terminated at the baffle ends by a single main chamber (refer to Figure 4).

Combustion and nozzle influences enter the problem as gain-loss boundary conditions. The combustion is assumed to be concentrated at the injector face. Support for this assumption is based upon experimental observation that the majority of the combustion processes are completed very near the injector of the chamber.[13] This model for the combustion also overestimates the energy input to the flow and thus represents the worst condition for stability.[14] The unsteady model for combustion mass generation used here is assumed to be only pressure dependent according to the Crocco n-τ time lag theory.[15]

On the opposite end of the chamber is a "short", quasi-steady nozzle. Due to the restrictive nature of the flow within this nozzle

a constant Mach number condition exists at its entrance.[16] The choice of this loss boundary condition has a secondary importance in this problem because the nozzle produces a minor damping influence.

Periodic oscillations are treated for a thermally and calorically perfect gaseous flow. The concentrated combustion assumption permits the gas dynamic flow field to be represented as a single constituent, product gas with no heat transfer or diffusion processes taking place. The core flow within the chamber is characterized by a constant Mach number steady flow and is devoid of molecular viscosity and turbulence effects. Consequently it is consistent to assume a velocity potential exists for the core main flow. Corrections to these assumptions are made by making boundary layer adjustments at the appropriate surfaces.

One final assumption is made with regard to this solution. Entropy variations are neglected in this analysis. This assumption is consistent with the small overall influence they produce on the problem.[17]

Before mathematically describing the preceeding flow, a nondimensionalization of the thermodynamic variables and the velocity field with respect to the steady state values is made. Because of the concentrated combustion assumption, the steady state thermodynamic variables and gas velocity are spatially independent and are represented as constants.

The nondimensional conservation equations governing the flow are given in the following relationships. The conservation of mass has the form:

$$\frac{D\rho}{Dt} + \rho\vec{\nabla}\cdot\vec{q} = 0$$

where ρ and $\vec{q}$ are the density and gas velocity. These quantities are nondimensionalized as:

$$\rho = \rho^*/\bar{\rho}^*$$

$$\vec{q} = \vec{q}^*/\bar{a}^*$$

where $\bar{a}^*$ is the dimensional steady state speed of sound. The independent variables z, y and t are nondimensionalized as:

$$y = y^*/R^*$$

$$z = z^*/R^*$$

$$t = t^*\bar{a}^*/R^*$$

In this two dimensional chamber R^* refers to a characteristic length along y^*.

The momentum equation is:

$$\rho \frac{D\vec{q}}{Dt} + \frac{1}{\gamma} \vec{\nabla} P = 0$$

where P is the nondimensional pressure given as $P = P^*/\bar{P}^*$ and γ is the ratio of the specific heats.

The final relationship is the homentropic condition:

$$P = \rho^{\gamma}$$

The velocity potential assumption allows the velocity field to have the following representation:

$$\vec{q} = \vec{\nabla} \phi$$

The state variables are then represented as power series expansions in an amplitude parameter (ε), i.e.

$$\phi = \bar{\phi} + \varepsilon \phi' + O(\varepsilon^2)$$

$$P = 1 + \varepsilon P' + O(\varepsilon^2)$$

With these expansions a first order linearization of the conservation equations is made which yields the following equations:

$$P' = \gamma \rho'$$

$$\nabla^2 \phi' - \frac{\partial^2 \phi'}{\partial t^2} = 2M \frac{\partial^2 \phi'}{\partial z \partial t} + M^2 \frac{\partial^2 \phi'}{\partial z^2} \tag{1}$$

$$P' = -\gamma \left[\frac{\partial \phi'}{\partial t} + M \frac{\partial \phi'}{\partial z} \right] \tag{2}$$

Since standing wave solutions are examined in this analysis it is consistent to assume exponential time dependence of the perturbations. Therefore the perturbed pressure and velocity potential have the forms:

$$P' = P(\vec{R}) e^{i\omega t} \quad \text{and} \quad \phi' = \phi(\vec{R}) e^{i\omega t}$$

where $\omega = \omega_r + i\lambda$ is the complex frequency and λ is the decay rate. Substitution of this time dependence transforms equations 1 and 2 into the following forms:

$$\nabla^2 \phi + \omega^2 \phi = 2i\omega M \frac{\partial \phi}{\partial z} + M^2 \frac{\partial^2 \phi}{\partial z^2} \tag{3}$$

$$P = -\gamma \left[i\omega \phi + M \frac{\partial \phi}{\partial z} \right] \tag{4}$$

The gain-loss boundary conditions at the injector and nozzle entrance surfaces are formulated, respectively, with the aid of Crocco's n-τ time lag theory and the "short" nozzle approximation. The combustion boundary condition is mathematically expressed as:

$$\dot{m}' = \bar{\dot{m}} n \left\{ P'(t) - P'(t - \bar{\tau}) \right\}$$

or

$$\left. \frac{\partial \phi}{\partial z} \right|_{z=0} + \left. \frac{MP}{\gamma} \right|_{z=0} = M n (1 - e^{-i\omega\bar{\tau}}) \left. P \right|_{z=0} \tag{5}$$

where n is the interaction index, (a measure of the amplitude dependence of the mass generation on the pressure), and $\bar{\tau}$ is the sensitive time lag, (a time phasing of the mass generation with the pressure). Typical values for n and $\bar{\tau}$ take the following ranges:[18]

$$0.14 \leq \bar{\tau}^{*} \leq 0.20 \text{ millisecs}$$

$$0.6 \leq n \leq 0.8$$

The "short" nozzle (constant entrance Mach number) approximation allows a loss boundary condition which is expressed mathematically as:

$$\left.\frac{\partial \phi}{\partial z}\right|_{z=L} = M\frac{(\gamma-1)}{2\gamma} \left. P\right|_{z=L} \tag{6}$$

On the remaining surfaces of the chamber and on the baffle blade surfaces hard wall boundary conditions are used. This is expressed by a zero normal component of velocity.

With the partial differential equation for the first order velocity potential and the linearized boundary conditions a solution is then obtained. Because of the discontinuous geometry of the problem, a separation of variables solution can not be directly obtained and a more sophisticated method is necessary. This method calls for separate solutions in the baffle cavities and the main chamber. A matching of these solutions is made at an artifical interface between these regions thus producing the complete solution.

The solution within the baffle cavities ($0 \leq z \leq z_B$) is found by separation of variables and utilizes the injector and hard wall boundary conditions. This solution takes the form:

$$\varphi = \sum_{m=0}^{\infty} A_m^{\mu} \cos m\pi y \left[\frac{e^{iB_1 z} + C_B e^{iB_2 z}}{e^{iB_1 z_B} + C_B e^{iB_2 z_B}}\right] \tag{7}$$

where N is the total number of baffle cavities and μ is an integer which defines a particular baffle compartment for $\frac{\mu-1}{N} \leq y \leq \mu/N$ (refer to Figure 4). The constants $B_{1,B}$, $B_{2,B}$ and C_B are defined by the differential equation and the boundary conditions. (These constants are explicitly defined in the Appendix.)

Within the main chamber ($z_B \leq z \leq L$) the perturbed velocity potential takes the form

$$\phi^c = \sum_{m=0}^{\infty} B_m \cos m\pi y \left[\frac{e^{iB_{1,c}(z-L)} + C_c e^{iB_{2,c}(z-L)}}{e^{iB_{1,c}(z_B-L)} + C_c e^{iB_{2,c}(z_B-L)}} \right] \qquad (8)$$

where $B_{1,c}$, $B_{2,c}$ and C_c are constants defined by the differential equation and the nozzle boundary condition. (These constants are given in the Appendix.)

The complete solution is then obtained by determining the proper set of $\{A_m^\mu\}$ and $\{B_m\}$. The continuity of axial velocity and velocity potential at the main chamber-baffle compartment interface produce the conditions necessary for the specification of the eigenfunction coefficients.

With the aid of the orthogonality properties of the series the following matching equations are obtained:

$$A_m^\mu = \sum_{m'=0}^{\infty} B_{m'} \frac{\int_{(\mu-1)/N}^{\mu/N} \cos m\pi Ny \cos m'\pi y \, dy}{\int_{(\mu-1)/N}^{\mu/N} \cos^2 M\pi Ny \, dy} \qquad (9)$$

and

$$B_m \left\{ \frac{iB_{1,c}\, e^{iB_{1,c}(z_B-L)} + iB_{2,c}\, C_c\, e^{iB_{2,c}(z_B-L)}}{e^{iB_{1,c}(z_B-L)} + C_c\, e^{iB_{2,c}(z_B-L)}} \right\} =$$

$$\sum_{m=0}^{\infty} \left\{ \frac{iB_{1,B}\, e^{iB_{1,B}z_B} + iB_{2,B}\, C_B\, e^{iB_{2,B}z_B}}{e^{iB_{1,B}z_B} + C_B\, e^{iB_{2,B}z_B}} \right\} \times$$

$$\sum_{\mu=1}^{N} A_m^{\mu} \frac{\int_{(\mu-1)/N}^{\mu/N} \cos m'\pi y \cos m\pi N y \, dy}{\int_0^1 \cos^2 m'\pi y \, dy} \qquad (10)$$

Equation 9 is the representation of the matching of velocity potential and Equation 10 is the matching of axial velocity at $z=z_B$. It is recognized that the solution to this problem satisfies a homogeneous differential equation with homogeneous boundary conditions and as such poses an eigenvalue problem. Since the amplitude is arbitrary in this solution, a normalization to a particular mode within the main chamber is made. This gives an additional relationship that is used to compute the eigenvalue (frequency). Mathematically this is expressed as:

$$B_{\hat{m}} = 1$$

or

$$\left\{ \frac{iB_{1,c}\, e^{iB_{1,c}(z_B-L)} + iB_{2,c}\, C_c\, e^{iB_{2,c}(z_B-L)}}{e^{iB_{1,c}(z_B-L)} + C_c\, e^{iB_{2,c}(z_B-L)}} \right\} =$$

$$\sum_{m=0}^{\infty} \left\{ \frac{iB_{1,B}\, e^{iB_{1,B}z_B} + iB_{2,B}\, C_B\, e^{iB_{2,B}z_B}}{e^{iB_{1,B}z_B} + C_B\, e^{iB_{2,B}z_B}} \right\} \times$$

$$\sum_{\mu=1}^{N} A_m^{\mu} \frac{\int_{(\mu-1)/N}^{\mu/N} \cos \hat{m}\pi y \cos m\pi N y \, dy}{\int_0^1 \cos^2 \hat{m}\pi y \, dy} \tag{11}$$

where $\hat{m}$ refers to the dominating transverse mode in the main chamber.

A successive approximation technique is used to solve Equations 9, 10 and 11. The first approximation chosen for this method uses the unbaffled chamber velocity potential solution, i.e. $B_m = \delta_{m,\hat{m}}$. With this approximation a calculation of the baffle compartment coefficients $\left\{A_m^{\mu}\right\}$ is made using Equation 9. These coefficients, in turn, are used to recalculate the main chamber coefficients $\left\{B_m\right\}$ from Equation 10 and the eigenvalue Equation 11. The procedure is then repeated until convergence is obtained. This iteration scheme converges very quickly and produces frequency predictions which have less than 5% differences after approximately 5 iterations.

In investigating the convergence of this solution, the matching relationships are checked by examining the velocity potential and axial velocity predictions at the interface ($z=z_B$). Figures 5 and 6 show these plots for a two and three compartment baffle configuration. With the use of Cesaro summation of the series expansions, reasonable agreement is obtained to assure correctness of the mathematics. These figures also indicate large velocities at the baffle blade tips ($z=z_B$). At these regions the eigenfunction expansions fail to accurately represent the flow field.

It is then necessary to characterize the velocity field near the baffle blade tips. To treat this problem a polar coordinate system is

set up at the blade tips and an expansion of the velocity potential is obtained (refer to Figure 7 for the coordinate system).

The partial differential equation describing the unsteady flow near the tips, Equation 3, is transformed into the following equation:

$$\left[\frac{\partial^2\phi}{\partial\zeta^2} + \frac{1}{\zeta}\frac{\partial\phi}{\partial\zeta} + \frac{1}{\zeta^2}\frac{\partial^2\phi}{\partial\alpha^2}\right] + \omega^2\phi = 2i\omega M\left[\frac{\mathrm{Sin}\alpha}{\zeta}\frac{\partial\phi}{\partial\alpha} - \mathrm{Cos}\alpha\frac{\partial\phi}{\partial\zeta}\right] + M^2\left[\mathrm{Cos}^2\alpha\left(\frac{\partial^2\phi}{\partial\zeta^2} + \frac{1}{\zeta}\frac{\partial\phi}{\partial\zeta} + \frac{1}{\zeta^2}\frac{\partial^2\phi}{\partial\alpha^2}\right) - \mathrm{Cos}2\alpha\left(\frac{1}{\zeta^2}\frac{\partial^2\phi}{\partial\alpha^2} + \frac{1}{\zeta}\frac{\partial\phi}{\partial\zeta}\right) + \mathrm{Sin}2\alpha\left(\frac{1}{\zeta}\frac{\partial^2\phi}{\partial\zeta\partial\alpha} - \frac{1}{\zeta^2}\frac{\partial\phi}{\partial\alpha}\right)\right]$$

The blade boundary conditions are represented as

$$\left.\frac{\partial\phi}{\partial\alpha}\right|_{\alpha=0,2\pi} = 0$$

If a proper ordering of the solution is made with respect to an asymptotic form, i.e.

$$\phi = \zeta^s A(\alpha) + k$$

where $0 \leq \zeta << 1$ and $s \geq 0$, it is found that the mean flow corrections (right hand side of above partial differential equation) are of the orders $O(\zeta M)$ and $O(M^2)$. Also the $\omega^2\phi$ term on the opposite side of the equation is a term of $O(\zeta^2)$. These terms are very small and are neglected to produce the asymptotic solutions:

$$\phi = a\,\zeta^{\frac{1}{2}}\,\mathrm{COS}\alpha/2 + k + O(\zeta) \qquad \zeta << 1 \qquad (12)$$

This solution indicates the singular behavior of the velocity field, i.e. $\partial\phi/\partial\zeta \to \infty$ and $1/\zeta\ \partial\phi/\partial\alpha \to \infty$, $\zeta \to 0$. The constants a and k are

determined by matching this asymptotic solution at some ζ_c with the outer eigenfunction expansions. Proper choice of ζ_c is made so that the remainder terms of Equation 12 are negligible and a region of proper matching of the outer expansions is realized.

Since only two match points are needed for this inner solution, the asymptotic expansion and the outer series expansions for the range encircling the blade tip are checked for consistency. Figure 8 shows this comparison. The velocity potential is well represented by this asymptotic expansion particularly for $\pi/2 \leq \alpha \leq 3\pi/2$. The differences at the other parts of the range are immediately accounted for by recognizing that the series expansions have outer boundary conditions. This, however, is not of major concern (as will be explained later) since the region of interest is $\pi/2 \leq \alpha \leq 3\pi/2$.

With this representation of the strong flow near the baffle tips, a calculation of energy dissipation due to molecular viscosity and turbulence is then made. Boundary layer corrections on the velocity are necessary. This correction for a laminar, periodic flow is given as:[19]

$$U(\vec{R},t)=U(\eta=\delta,t)(1-e^{-\delta_o \eta}) \qquad (13)$$

$$\delta_o=(1+i)\sqrt{\omega/2\mu_\nu}$$

where $U(\eta=\delta,t)$ is the periodic outer flow transverse velocity and η is the normal component to the boundary surface (refer to Figure 9).

An estimate of the mechanical energy dissipation within the boundary layer volume is then calculated from the following integral:[20]

$$E_{dis} \cong \int_{\Psi_{B.L.}} \mu_\nu \left(\frac{\partial U}{\partial \eta}\right)^2 \, d\eta dS \cong \gamma \int_S \sqrt{\frac{\mu_\nu \omega}{2}}\, U^2(\eta=\delta,t)\, dS \qquad (14)$$

Steady flow corrections are neglected in this calculation since these corrections are an order of magnitude smaller than the unsteady flow velocities. This is also consistent with the neglect of dissipation on the chamber walls.

A time average of the above relationship will then physically represent an average quantity of mechanical energy that is transformed irreversible into heat.

With the presence of combustion a highly turbulent flow situation must be realized and the existence of turbulence produces more energy dissipation.[21] To account for this dissipation, the Boussinesq approximation is retained which uses a stress-strain law for the time averaged turbulent flow. A "turbulent viscosity" which is a function of the local flow conditions is then necessary for the model. Many relationships exist for this parameter, each having limited applicability.[22] These relationships require a steady flow (apart from the turbulent fluctuations) far from the boundary surface. Models incorporating unsteady outer flow are nonexistent and must be created from existing steady flow theories. An effective viscosity model created by Spalding[23] is used for this analysis. This model is chosen because of its simplicity and its qualitative accuracy with respect to other combustion flow problems.[24] This model is represented as:

$$\mu^*_{eff} \propto \rho^{*2/3} \left(\dot{m}^*_F U^{*2}_F + \dot{m}_0 U^{*2}_0\right)^{1/3}$$

where the F and 0 subscript refer to the fuel and oxidizer quantities. In order to be consistent with the single component gas assumption of this problem, the fuel and oxidizer velocities are assumed to be uniform with the product gas velocity, i.e. $U^*_F = U^*_0 = U$ then the

equation reduces to:

$$\mu^*_{eff} \propto \rho^* |U^*|$$

where $|U^*|$ is a r.m.s. value of speed in the entire turbulent field.

An incorporation of the periodic flow velocity into the model is then made by time averaging the r.m.s. $|U^*|$ to give the final form of μ_{eff}:

$$\mu_{eff} = C_{turb} \left\{ M^2 + \varepsilon^2 \frac{U'\overline{U'}}{2} \right\}^{\frac{1}{2}} \tag{15}$$

Geometrical corrections to this equation are neglected since they have a weak dependence in the model. Spalding suggests a proportionality constant (C_{turb}) of the order O(0.05).

This model is then used to calculate the turbulent dissipation. By assuming that the turbulent velocity profiles are similar to the laminar predictions given by Equation 13, the following integral relation for the dissipation is obtained:[25]

$$E^T_{dis} \cong \int_{S_B} \gamma \sqrt{\frac{\mu_{eff}\omega}{2}}\, U^2 dS \tag{16}$$

The importance of the exactness of the turbulent velocity profile is secondary since a global, integral quantity is evaluated. However, it is experimentally observed that turbulent profiles are steeper in shape than the laminar flow profiles and consequently this dissipation calculation could be underestimated.

One final correction is necessary for the dissipation calculation. A physically impossible infinitely thin baffle blade will create an infinite amount of energy loss because of the singular behavior of the velocity at the tip. A baffle blade of finite thickness will therefore be used in this problem.

To correct for this thickness a neighboring streamline is used to represent the baffle surfaces. This eliminates a reworking of the solution to correct for the baffle shape since the normal component of velocity vanishes along a streamline. Figure 10 shows a streamline plot of the flow within a baffled chamber with no mean flow. Near the tips of the blades the streamlines are well represented by $\psi = \zeta^{\frac{1}{2}} \sin\alpha/2$ particularly for $\zeta << 1$ and $\pi/2 \leq \alpha \leq 3\pi/2$. This range defines the geometry of the blade tips. This streamfunction is retained to describe the rest of the baffle blade surface but because the velocity decreases substantially away from the blade tips this surface description is of secondary importance in the dissipation calculation. Mathematically this surface is represented as:

$$\zeta^{\frac{1}{2}} \sin\alpha/2 = (T/4)^{\frac{1}{2}}$$

where T is the blade thickness.

A calculation of the tip loss is now available using Equations 12, 15 and 16. Rather than correcting boundary conditions to account for this dissipation, as is done in acoustic theory, a more direct method of stability prediction is applied. An integral time average of the energy equation, derived by Cantrell and Hart,[26] is used to estimate the global stability of the flow within the combustor. Stability behavior (a calculation of decay rate of the perturbations) is examined by accounting for the energy inputs or extractions at the various surfaces of the chamber. Mathematically this relationship, correct to $O(\varepsilon^2)$, is stated as:

$$2\lambda \left\langle \int_V \left\{ \frac{P'^2}{2\gamma} + \frac{\gamma}{2} \vec{q}' \cdot \vec{q}' + MU'P' \right\} dV \right\rangle$$

$$= \left\langle \oint_S \left\{ P' \vec{q}' + \frac{P'^2}{\gamma} M \vec{e}_k \right\} \cdot d\vec{S} \right\rangle \qquad (17)$$

where λ is the decay rate that is of the order $0(\epsilon)$.

Evaluating the r.h.s. over the baffle surfaces results in a term representing the mechanical energy extracted at the surface. This can directly be equated to the dissipation integral Equation 16. By applying the appropriate boundary conditions the Cantrell and Hart integral relationship has the final form:

$$\lambda = \left\{ - \int_{Sinj} \frac{Mn(1-\cos\omega\bar{\tau})}{2} \overline{P'P'} \, dSinj + \int_{S_{noz}} \frac{M(\gamma+1)}{2\gamma} \frac{\overline{P'P'}}{2} dS_{noz} \right.$$

$$\left. + \int_\gamma \sqrt{\frac{\mu_{eff}\omega}{2}} \frac{\overline{U'U'}}{2} dS_B \right\} \Big/ \left\{ \int_V \left[\frac{\overline{P'P'}}{2\gamma} + \frac{\gamma}{2} \overline{\vec{q}' \vec{q}'} \right] dV \right\} \qquad (18)$$

The first term in the numerator represents the energy added to the unsteady flow by the combustion, the second term the energy extracted by the nozzle, and the third term the energy loss created by the strong flow surrounding the baffle blade tips.

Stability calculations using this mathematical analysis are coded in Fortran and evaluated using a CDC 6400 computer. Inputs to the program include combustor geometry, baffle configuration, mea flow Mach number and oscillation mode character. Some aspects of the computation problem are discussed later.

Section III

THEORY--THREE DIMENSIONAL CHAMBER

A more realistic description of the problem of interest is made by discarding the two dimensional geometry assumption and treating a three dimensional cylindrical combustion chamber. The baffles enter the geometry in a similar manner by dividing the injector end of the chamber into equal angle sector compartments (refer to Figure 11).

Since the same partial differential equation and boundary conditions are applied to this problem, the extention to the three dimensional problem requires doubly infinite eigenfunction expansions in the main chamber and baffle compartments. These expansions are as follows:

$$\phi^C = \sum_{m=0}^{\infty}\sum_{\ell=1}^{\infty} B_{\ell m}\ \Psi^C_{\ell m}(r,\theta)\left\{\frac{e^{iB_{1,C}(z-L)} + e^{iB_{2,C}(z-L)}}{e^{iB_{1,C}(z_B-L)} + C_C\, e^{iB_{2,C}(z_B-L)}}\right\} \qquad (19)$$

and

$$\phi^B = \sum_{m=0}^{\infty}\sum_{\ell=1}^{\infty} A_{\ell m}\ \Psi^B_{\ell m}(r,\theta)\left\{\frac{e^{iB_{1,B}z} + C_B\, e^{iB_{2,B}z}}{e^{iB_{1,B}z_B} + C_B\, e^{iB_{2,B}z_B}}\right\} \qquad (20)$$

where

$$\Psi^B_{\ell m}(r,\theta) = \frac{\cos mN\theta}{2}\ J_{\frac{mN}{2}}(\lambda^B_{\ell m} r) \qquad \frac{2\pi(j-1)}{N} \leq \theta \leq \frac{2\pi j}{N}$$

Within the main chamber two types of solution are possible. The standing wave solution is made by specifing:

$$\Psi^C_{\ell m}(r,\theta) = \cos m\theta\ J_m(\lambda^C_{\ell m} r)$$

The traveling wave solution is given by:

$$\psi^{c}_{\ell m}(r,\theta) = e^{im\theta} J_m(\lambda^{c}_{\ell m} r)$$

The constants $B_{1,B}$, $B_{2,B}$, C_B, $B_{1,c}$, $B_{2,c}$ and C_c are given explicitly in the Appendix.

The matching relationships and eigenvalue equation that are necessary in obtaining a complete solution take the following forms:

$$A^{\mu}_{\ell m} = \sum_{m'=0}^{\infty}\sum_{\ell'=1}^{\infty} B_{\ell' m'} \frac{\int_{\frac{2\pi(\mu-1)}{N}}^{\frac{2\pi\mu}{N}}\int_{0}^{1} \psi^{B}_{\ell m}(r,\theta)\, \psi^{C}_{\ell' m'}(r,\theta)\, r\,dr\,d\theta}{\int_{\frac{2\pi(\mu-1)}{N}}^{\frac{2\pi\mu}{N}}\int_{0}^{1} \psi^{B^2}_{\ell m}(r,\theta)\, r\,dr\,d\theta}$$

and

$$\delta_{\ell' m'}\left\{\frac{iB_{1,c}\, e^{iB_{1,c}(z_B-L)} + iB_{2,c}\, C_c\, e^{iB_{2,c}(z_B-L)}}{e^{iB_{1,c}(z_B-L)} + C_c\, e^{iB_{2,c}(z_B-L)}}\right\} =$$

$$\sum_{m=0}^{\infty}\sum_{\ell=1}^{\infty}\left\{\frac{iB_{1,B}\, e^{iB_{1,B}z_B} + iB_{2,B}\, C_B\, e^{iB_{2,B}z_B}}{e^{iB_{1,B}z_B} + C_B\, e^{iB_{2,B}z_B}}\right\} \times$$

$$\left\{\sum_{\mu=1}^{N} A^{\mu}_{\ell m} \frac{\int_{\frac{2\pi(\mu-1)}{N}}^{\frac{2\pi\mu}{N}}\int_{0}^{1} \psi^{B}_{\ell m}(r,\theta)\, \overline{\psi^{C}_{\ell' m'}}(r,\theta)\, r\,dr\,d\theta}{\int_{0}^{2\pi}\int_{0}^{1} \psi^{C}_{\ell' m'}(r,\theta)\, \overline{\psi^{C}_{\ell' m'}}(r,\theta)\, r\,dr\,d\theta}\right\}$$

The eigenvalue equation is represented as:

$$B_{\ell m} = 1$$

or

$$\left\{ \frac{iB_{1,c}\, e^{iB_{1,c}(z_B-L)} + iB_{2,c}\, C_c\, e^{iB_{2,c}(z_B-L)}}{e^{iB_{1,c}(z_B-L)} + C_c\, e^{iB_{2,c}(z_B-L)}} \right\} =$$

$$\sum_{m=0}^{\infty}\sum_{\ell=1}^{\infty}\left\{ \frac{iB_{1,B}\, e^{iB_{1,B}z_B} + iB_{2,B}C_B\, e^{iB_{2,B}z_B}}{e^{iB_{1,B}z_B} + C_B\, e^{iB_{2,B}z_B}} \right\}$$

$$\left\{ \sum_{\mu=1}^{N} A_{\ell m}^{\mu} \frac{\int_{\frac{2\pi}{N}(\mu-1)}^{\frac{2\pi\mu}{N}} \int_0^1 \Psi_{\ell m}^{B}(r,\theta)\, \overline{\Psi_{\hat{\ell}\hat{m}}^{C}(r,\theta)}\, r\,dr\,d\theta}{\int_0^{2\pi}\int_0^1 \Psi_{\hat{\ell}\hat{m}}^{C}(r,\theta)\, \overline{\Psi_{\hat{\ell}\hat{m}}^{C}(r,\theta)}\, r\,dr\,d\theta} \right\}$$

where $\hat{m}$ and $\hat{\ell}$ respectively specifies the dominating transverse and radial modes in the main chamber.

An initial approximation to the preceeding equation sets is similar to the two dimensional chamber problem and is given by

$$B_{\ell m} = \delta m,\hat{m}\ \delta \ell,\hat{\ell}$$

The same iteration scheme described in the previous chapter is then used to obtain higher approximations.

Figure 12 shows a comparison of the matching of the velocity potential and the axial velocity at the baffle compartment-main chamber interface. Reasonable agreement of the matchings as predicted by the baffle compartment solution as compared to the main chamber solution indicates the correctness of the solution method. Also indicated is the singular behavior of the velocity field at the baffle tips.

An asymptotic expansion is used to describe the velocity potential near the tips with the allowance of radial dependence of the parameters

a and k in Equation 12. With this solution the energy dissipation given by Equation 16 is used with the Cantrell-Hart stability Equation 18 to predict decay rate.

A Fortran program is used to analyze the results of the calculations with the inputs of combustor geometry, baffle configuration, mean flow Mach number, and main chamber mode character. Computation is more lengthy in the three dimensional problem and requires 20 times the computer time required for the two dimensional chamber problem. The next section gives some details concerning the computational problems involved.

Section IV

COMPUTER SOLUTION

Several aspects of the computer evaluation of the preceeding solutions merit further explanation. First, convergence of the solution with respect to approximating the infinite series expansions and the iteration method used to calculate these expansions is discussed. A major concern in this solution is the accuracy of the velocity potential representation.

In the two dimensional chamber solution, the number of terms used to approximate the infinite series is not a critical problem because the solution is represented as a single series expansion that requires relatively little computing time. Typically a 30 term expansion in the baffle compartments and main chamber produced sufficient agreement of the match of the velocity potential at the baffle compartment-main chamber interface. This number of terms is also sufficient for the match of the baffle compartment series solution to the asymptotic solution near the blade tips. Increasing the number of terms has only a slight effect on the overall model predictions, decreasing the number of terms causes only a modest reduction in computer time required.

Compared with the two dimensional chamber solution, the three dimensional cylindrical chamber solution is more complex. The complications of calculating the solution arise from the double infinite Fourier-Bessel expansions by which the solution is represented. The number of terms used to approximate these infinite expansions is very critical and drastically influences computing time and storage. Improved convergence and the elimination of Gibbs phenomena has been

attained using Cesáro summation.[27] The use of this technique allows a reduction in the number of terms retained in the expansions and computing time is consequently reduced. Figure 13 shows a comparison of the baffle compartment and main chamber series solutions of the axial velocity at the baffle-main chamber interface ($z=z_b$). These 10 term expansions (summed without the Cesáro technique) are grossly matched. Figure 14 shows the improvement of the matching with the application of Cesárc summation to the series solutions.

The second aspect of convergence is concerned with the iteration scheme used to solve the matching relationships and the eigenvalue equation. This is not a major problem because the successive approximation technique converges very quickly. Typically after 5 iterations the frequency predictions differ between successive iterations by less than 5%. However, the eigenvalue equation has multiple solutions so care must be taken in choosing the proper initial frequency.

In arriving at the solutions several integral quantities are numerically evaluated using an improved quadrature method. Eleven quadrature modes evaluate the dissipation integral with sufficient accuracy. Another integral quantity is evaluated using eleven quadrature nodes and appears in the cylindrical chamber matching relationships:

$$\int_0^1 J_{\frac{mN}{2}}(\lambda_{\frac{mN}{2}} r)\; J_{m'}(\lambda_{\frac{m'N}{2}} r)\; r\,dr$$

A matrix of these integrals is evaluated numerically and represents a major part of the computing and storage of the computer program. For

large values of $\lambda_{\ell,mN/2}$ and $\lambda_{\ell',m'}$ more quadrature modes must be used to assure proper convergence of the solution.

Typical computation times for a particular baffle configuration (and consequently one ω_R and λ) are 60 seconds for the two dimensional chamber solution with 30 term expansions and 1000 seconds for the three dimensional chamber solution which uses 10x10 Fourier-Bessel expansion for the solution. Better optimization and storage could possibly reduce these computing requirements.

Section V

RESULTS

Previous investigations based on wave alteration as the possible mechanism for the damping produced by baffles have failed to correctly predict stability trends. These studies have all neglected viscous and turbulence effects in the flow. The incorporation of these effects is of major importance in this problem and is necessary to describe the stability behavior of baffled combustors.

Before discussing results from the present model which uses mechanical energy dissipation as a damping mechanism, the shortcomings of previous analytical attempts will be clarified. A well established criterion stated by Lord Rayleigh clearly indicates why wave alteration may cause a destabilizing behavior in baffled combustors. The sense of the criterion is given by Rayleigh's statement, "If heat be given to the air at the moment of greatest condensation, or be taken from it at the moment of greatest rarefraction the vibration is encouraged."[12] A mathematical formulation of this statement has been made by Cantrell and Hart and is given by Equation 17 in Section II. Applying the appropriate boundary conditions on the injector surface, S_{inj}, and on the nozzle entrance surface, S_{noz}, allows an integral inequality which can be used to predict the global stability of the perturbed contined flow. By referencing the combustion parameter n and $\bar{\tau}$ to those of an unbaffled neutrally stable combustor this inequality is reduced to a function of only the perturbed pressure distributions on the surfaces S_{inj} and S_{noz}. (In this reference chamber oscillations neither grow or decay with time because energy is added or extracted at the same

pressure level.) Formally, the inequality requires that for unstable oscillations:

$$\left\langle \int_{S_{inj}} P'^2 \, dS_{inj} \right\rangle \geq \left\langle \int_{S_{noz}} P'^2 \, dS_{noz} \right\rangle$$

In other words, if more energy is added due to the combustion than is extracted by the nozzle the flow is unstable. The equality sign indicates neutral stability behavior of the flow.

Figure 15 shows the pressure distribution for a baffled and unbaffled combustor at the nozzle (z=L) and injector (z=0) ends of the chamber. Without a baffle the combustor is neutrally stable and shows identical pressure distributions over injector and nozzle surfaces. Placement of a baffle in a chamber results in a pressure amplitude rise at the injector surface and a pressure amplitude loss at the nozzle. Consequently, the flow becomes unstable.

It is this pressure wave alteration which has resulted in earlier investigations predicting a destabilizing influence for baffles. Only with the consideration of mechanical energy dissipation will the stabilizing influence of baffles become apparent. Some results for the present model which includes this dissipative influence will now be discussed.

Two Dimensional Chamber Results

Linear stability predictions are examined first in a two dimensional combustor modeled as a rectangular chamber with a length L=1.5. First transverse mode oscillations are studied and are assumed to dominate the solution within the main chamber. (First transverse mode

refers to a standing oscillation in the y direction that has a half-cycle between y=0 and y=1.) The parameters n and $\bar{\tau}$ required for the unsteady combustion model are assigned the values $n=(\gamma+1)/4\gamma$ and $\bar{\tau}=1$. These choices are made so that a neutrally stable unbaffled combustor is referenced (i.e. with no baffles the chamber is neutrally stable).

For the dissipation model a value for the turbulent coefficient $C_{turb} = 0.034$ is used and is the value suggested by Spalding.[23] Also a nondimensional thickness which is typical of actual baffle configurations of T=0.05 is chosen for the baffle blades.

Before examining the stability trends, the effects of blade length on the normalized frequency, (frequency of the baffled chamber/frequency of the unbaffled chamber), are examined. Figure 16 shows that the frequency decreases when a baffle is added to a chamber. Furthermore, an increase in blade length further depresses the frequency. This prediction is in agreement with the experimental data provided by Aerojet-General.[6] Mean flow corrections to this frequency as predicted by the model are shown in Figure 17 It is seen that the normalized frequency is reduced with an increase in mean flow Mach number.

The principal result of these calculations is the prediction of combustor stability. Decay rates are calculated for various baffle blade lengths and chamber conditions. Decay in decibel/cycle is defined as follows:

$$\text{Decay in decibels/cycle} = 20 \log_{10}\left[\frac{P'(t)}{P'(t + 2\pi/\omega_r)}\right]$$

With the exponential time dependence of the oscillations in this problem this definition reduces to:

$$\text{Decay in decibels/cycle} = 54.575\ \lambda/\omega_R$$

where λ is the decay rate and ω_r is the frequency.

Figure 18 shows decay predictions for a two compartment baffle configuration in a two dimensional combustor with no mean flow (pure acoustic flow). Two wave amplitudes (ϵ) are examined and are shown to bracket the qualitative stability trends as reported in experimental observations (again from Aerojet-General data). With an increase in amplitude the combustor stability is improved. This improvement is attributed to the increased kinetic energy of the flow which increases the turbulent viscosity near the blade tips.

With the addition of combustion and nozzle influences in the flow, the flow field must contain mean flow corrections. These influences increase the energy densities of the flow and consequently increase the mechanical energy dissipation. However, the addition of combustion increases the energy input into the flow and lessens the global stability of the flow. Figure 19 shows the stability trends for a combustor experiencing oscillations with amplitude $\epsilon = 0.1$ for various mean flow Mach numbers. Even with the combustion input, sufficient dissipation exists to stabilize the chamber providing that the baffle blades are long enough. The effectiveness of increasing the blade length of the baffle is reduces as the mean flow Mach number is increased, providing the wave amplitude stays constant. Beyond a blade length $z_B = 0.1$ the nozzle virtually loses all its damping ability because the pressure oscillations are distorted so that a pressure node at the nozzle entrance occurs. Consequently, only the baffle tip dissipation remains to counteract the energy input at the injector. It can be seen in Figure 19 that for large Mach numbers a baffle can destabilize a combustor because the increased energy due to the combustion overpowers the energy loss at the blade tips. This may be an explanation for the

experimental observation that baffles can be too short and actually destabilize the combustor. However, it must be recognized that the concentrated combustion model overpredicts the energy input to the combustor and in doing so may be responsible for the destabilizing behavior. Also with an increase in combustion input into the chamber an increase in wave amplitude (ε) can be expected. This Mach number dependence in ε is neglected in the results of Figure 19 and consequently the dissipation is underestimated for large Mach numbers.

Stability trends for several baffle configurations are shown in Figure 20. Baffle configuration is seen to have a secondary influence in the problem. Adding more compartments to a configuration decreases the tip velocities and also increases the surface area. These influences counterbalance each other and produce small changes in stability character of baffle configuration. There is an advantage of large compartment configurations, however, since more modes can be effectively damped with many compartments. For example, a two compartment baffle is only effective in damping odd numbered transverse modes whereas a five compartment baffle is effective in damping all modes except those which are multiples of five.

Figure 21 shows the effectiveness of a two compartment baffle configuration in damping the first and third transverse mode in the main chamber (wave amplitude $\varepsilon = 0.1$). The third transverse mode characterizes a standing oscillation which has three half-cycles between $y = 0$ and $y = 1$. Figure 21 displays the fact that a baffle which damps the first transverse mode also damps the third transverse mode. The decibel rating of decay/cycle is misleading in this figure because the frequency scales are different. (The frequency of the third transverse

mode is about three times that of the first transverse mode.) A more representative stability plot is given in Figure 22 and is a plot of decay rate (λ) for various blade lengths. This figure indicates the similar behavior of the two cases.

Three Dimensional Chamber Results

Of greater practical interest are the stability predictions for the three dimensional cylindrical chamber model used in this work. A particular chamber with a length to radius ratio of $L/R = 1.5$ is examined. A three bladed, evenly spaced baffle configuration with blade thickness $T = 0.05$ is input into the dissipation model for the turbulent viscosity. Three dimensional first transverse mode oscillations in the main chamber are studied with an unsteady combustion input which use $n = (\gamma+1)/4\gamma$ and $\bar{\tau} = \pi/\lambda_{1,1}$. Again a neutrally stable unbaffled combustor is referenced with these parameters.

The frequency predictions of the three dimensional solution parallel those of the two dimensional solution and are in agreement with experimental data. These results are shown in Figure 23.

Decay rate predictions are shown in Figure 24 for a combustor with no mean flow and no combustion or nozzle influences. Two wave amplitudes, ($\varepsilon = 0.1$ and $\varepsilon = 0.2$) are shown in this figure and indicate the stabilizing behavior of baffles. Because of the additional radial dependence in the three dimensional chamber solution the baffle tip velocities are not as large as those predicted in the two dimensional chamber solution. Consequently, the dissipation is overestimated in the two dimensional chamber solution relative to the more realistic three dimensional chamber case.

Figure 25 shows the stability prediction of a cylindrical combustor which has a mean flow (M = 0.1), combustion and nozzle influences and is experiencing oscillations with amplitude $\varepsilon = 0.1$. Two types of oscillation are possible for this combustor: standing and traveling wave oscillations. Without dissipation influences, it is seen that these solutions produce the same destabilizing influence for the baffle (as predicted by the Rayleigh criterion). With the inclusion of mechanical energy dissipation in the model, these results are reversed and show a stabilizing influence for the baffle. It is seen that the traveling wave solution is most affected by the presence of the baffle and produces decay rates that are four times those of the standing wave solution. This is a critical result because the traveling wave is most common and is the most destructive. It is also apparent that the phasing between the oscillations in the main chamber and the standing wave oscillations in the baffle cavities produce different stability results. This observation is also made in Wieber's experimental results.[7]

Mean flow corrections to decay rate are shown in Figure 26. These predictions agree with the two dimensional chamber solutions and indicate that a particular baffle blade length becomes less effective with an increase in mean flow Mach number, providing ε is constant. Again the Mach number dependence of ε has been neglected from this result and as such underpredicts the dissipation for large Mach numbers.

The sensitivity of turbulent viscosity model to the selection of C_{turb} is the final parameter examined in this study. Figure 27 shows that an increase in C_{turb} gives an increase in decay rate. This parameter has been treated as having secondary importance since only

qualitative results can at this time be predicted. More reliable turbulence data is necessary to assure the proper model for the turbulent viscosity or a proper value of C_{turb}.

Section VI

CONCLUSIONS

A theoretical study of the stability of flows within combustion chambers with evenly spaced baffle configurations was presented. For the first time, a stabilizing influence for baffles has been properly predicted in an analytical model which incorporates the influences of a concentrated combustion source at the injector, a "short" nozzle terminating the chamber, and mechanical energy dissipation at the baffle blade tips. Two separate combustion chamber geometries are examined with this model and produce the following results:

1. The addition of a baffle to a combustor in many situations will improve the stability of a chamber.
2. A fluid dynamic loss created by the effects of viscosity and turbulence produce the damping mechanism of the baffle. This energy dissipation occurs locally at the baffle blade tips.
3. Without the effects of mechanical energy dissipation, wave alteration produced by the addition of a baffle to a combustor cause a destabilizing influence.
4. The baffle is most effective in damping the traveling transverse modes of oscillation.
5. An improvement in combustor stability is generally achieved with an increase in baffle blade length.
6. Longer baffles may be required for combustors which contain an increased mean flow.

7. The addition of a baffle to a combustion chamber depresses the oscillation frequency.
8. Baffle configuration has a secondary influence on the stability of the chamber.

BIBLIOGRAPHY

1. Zinn, B. T., Liquid Propellant Rocket Combustion Instability, edited by D. T. Harrje and F. H. Readon, NASA SP 194, 1972, Chap. 8.3.1, pp. 400-410.

2. Tonon, T. S., P. K. Tang, W. A. Sirignano and D. T. Harrje, "Acoustic Liner Design from a Fluid Mechanic Approach," AIAA/SAE 7th Propulsion Joint Specialist Conference, AIAA paper No. 71-757, June, 1971.

3. Mitchell, C. E., W. R. Espander and M. R. Baer, "Determination of Decay Coefficients for Combustors with Acoustic Absorbers," NASA CR-120836, 1972.

4. Male, T. and W. R. Kerslake, "A Method for Prevention of Screaming in Rocket Engines," NACA RM E54F28A, Aug. 1954.

5. McBride, J. M., Liquid Propellant Rocket Combustion Instability, edited by D. T. Harrje and F. H. Reardon, NASA SP 194, 1972, Chap. 8.2.3, pp. 395-399.

6. Reardon, F. H., Liquid Propellant Rocket Combustion Instability, edited by D. T. Harrje and F. H. Reardon, NASA SP 194, 1972, Chap. 3.5.3.3, pp. 156-159.

7. Wieber, P. R., "Acoustic Decay Coefficients of Simulated Rocket Combustors," NASA TN D-3425, May 1966.

8. Morse, P. M., and K. U. Ingård, Theoretical Acoustics, McGraw-Hill Book Co., Inc., New York, 1968, pp. 285-291.

9. Reardon, F. H., Liquid Propellant Rocket Combustion Instability, edited by D. T. Harrje and F. H. Reardon, NASA SP194, 1972, Chap. 8.2.1, pp. 386-389.

10. Sirignano, W. A., and W. C. Strahle, "A New Concept in Rocket Engine Baffles," AIAA Journal, Vol. 3, No. 5, May 1965, pp. 954-956.

11. Oberg, C. L., W. H. Evers and T. L. Wong, "Analysis of the Wave Motion in Baffled Combustion Chambers," NASA CR-72879, October 1971.

12. Rayleigh, Lord, The Theory of Sound, Vol. II, 2nd edition, Dover Publications, 1945, pp. 226.

13. Priem, R. J. and M. R. Heidmann, "Propellant Vaporization as a Design Criterion for Rocket Engine Combustion Chambers," NASA TR R-67, 1960.

14. Baer, M. R., C. E. Mitchell and W. R. Breander, "Stability of Partially Lined Combustors with Distributed Combustion," AIAA Journal, Vol. 12, No. 4, April 1974, pp. 475-480.

15. Crocco L. and S. I. Cheng, Theory of Combustion Instability in Liquid Propellant Rocket Motors, AGARDograph No. 8, Butterworths, 1956.

16. Crocco L. and W. A. Sirignano, "Effect of the Transverse Velocity Component on the Nonlinear Behavior of Short Nozzles," AIAA Journal, Vol. 4, No. 8, August 1966.

17. Mitchell, C. E., "The Effect of Entropy Waves on High Frequency Pressure Oscillations in Liquid Rocket Motors," Combustion Science and Technology, Vol. 1, 1970, pp. 269-274.

18. Reardon, F. H., Liquid Propellant Rocket Combustion Instability, edited by D. T. Harrje and F. H. Reardon, NASA SP194, 1972, Chap. 6.3, pp. 277-286.

19. Schlicting, H., Boundary Layer Theory, McGraw-Hill Book Co., 6th edition, 1968, pp. 411-427.

20. Landau, L. D. and E. M. Lifshitz, Fluid Mechanics, Pergamon Press, 1959, pp. 299-302.

21. Townsend, A. A., The Structure of Turbulent Shear Flow, Cambridge University Press, 1956.

22. Launder, B. E. and D. B. Spalding, Mathematical Models of Turbulence, Academic Press, 1972.

23. Gosman, A. D., W. M. Pun, A. K. Runchel, D. B. Spalding and M. Wolfshtein, Heat and Mass Transfer in Recirculating Flows, Academic Press, New York, 1969, pp. 207-212.

24. Tou, P. R. Russell and J. O'hara, "Experimental Determination of Turbulence in a GH_2 -GOX Rocket Combustion Chamber," NASA CR-134672, August 1974.

25. Schlicting H., Boundary Layer Theory, McGraw-Hill Book Co., 6th edition, 1968, p. 659.

26. Cantrell, R. H. and R. W. Hart, "Interaction Between Sound and Flow in Acoustic Cavities: Mass, Momentum and Energy Consideration," Journal of Acoustical Society of America, Vol. 36, No. 4, April 1964, pp. 697-706.

27. Evans, C. M., "Cesáro Summation of Series in Boundary-Value Problems," Journal of the Franklin Institute, Vol. 289, No. 3, March 1970, pp. 185-191.

28. Kronrod, A. S., Nodes and Weights of Quadrature Formulas. (Russian Translation) consultants Bureau, New York, 1965.

FIGURES

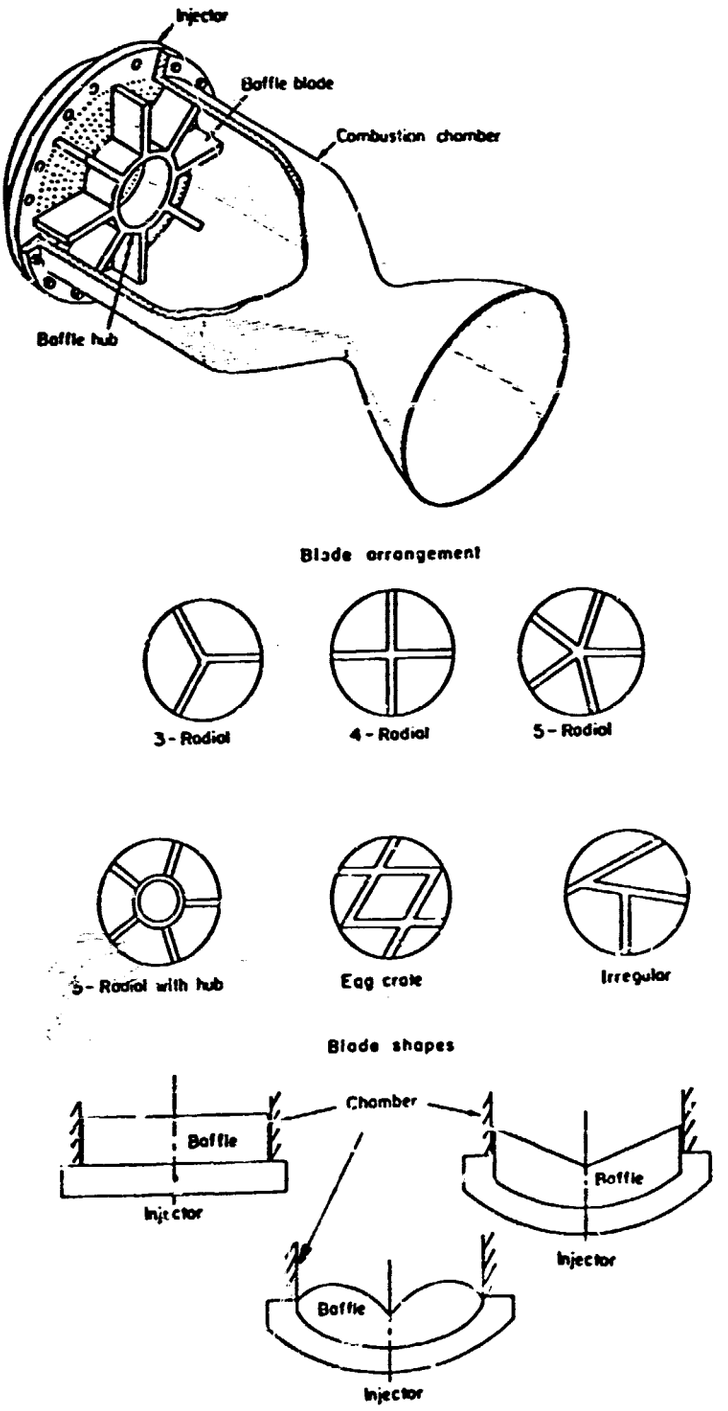

Figure 1. Several baffle configurations and baffle blade shapes.

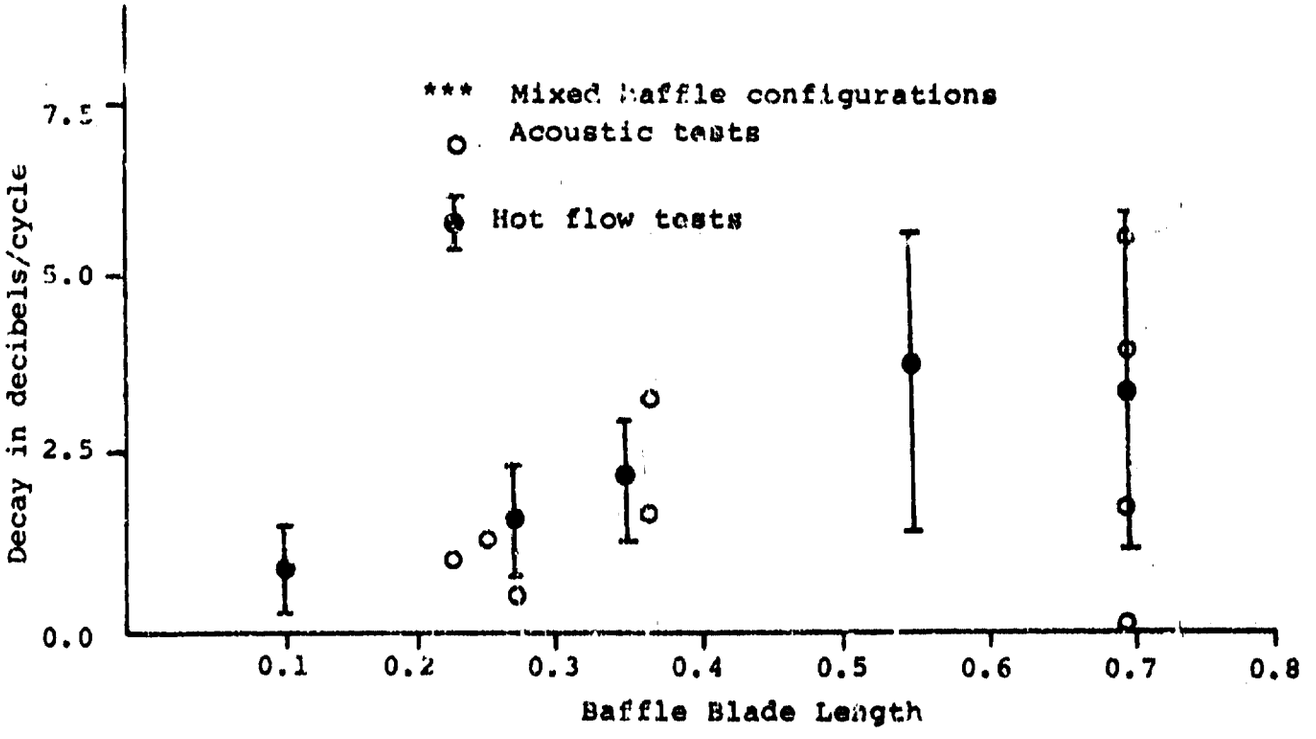

Figure 2. Aerojet-General experimental data of decay in decibels/cycle vs. baffle blade length.

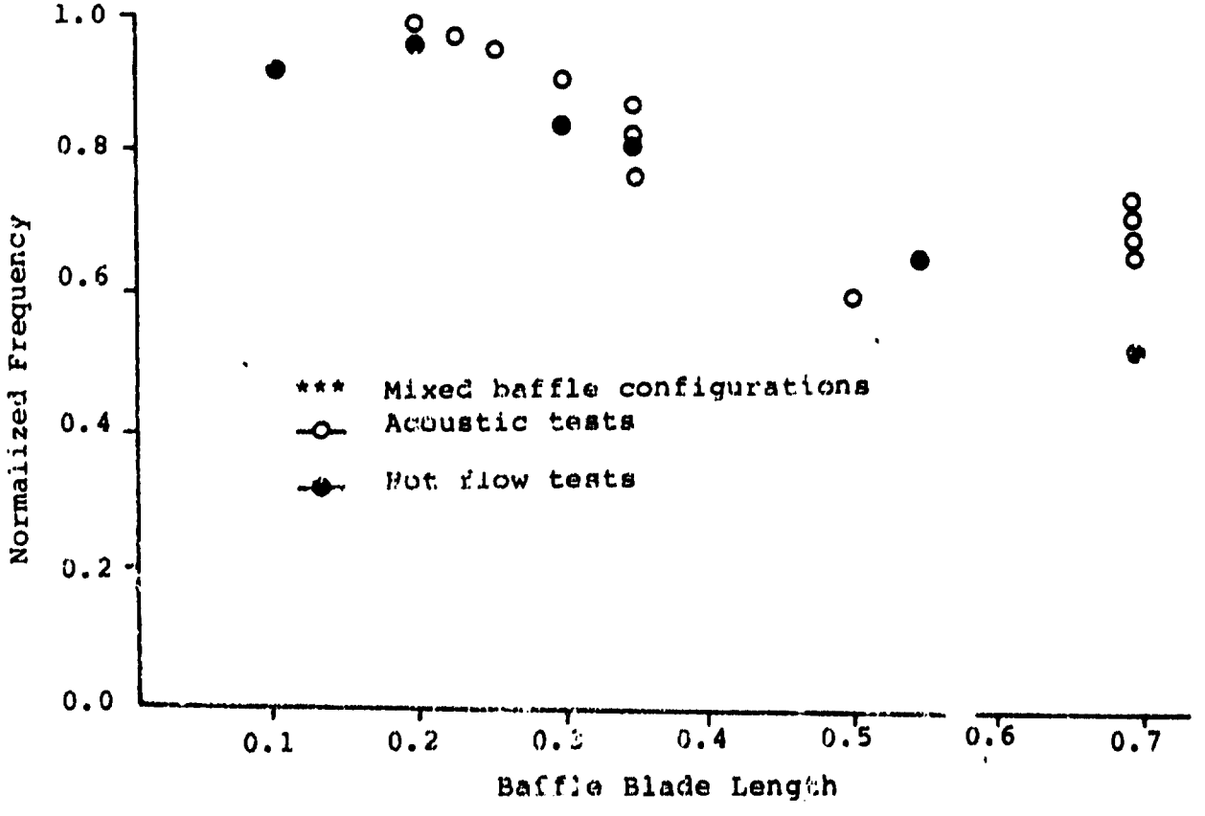

Figure 3. Aerojet-General experimental data of normalized frequency vs. baffle blade length.

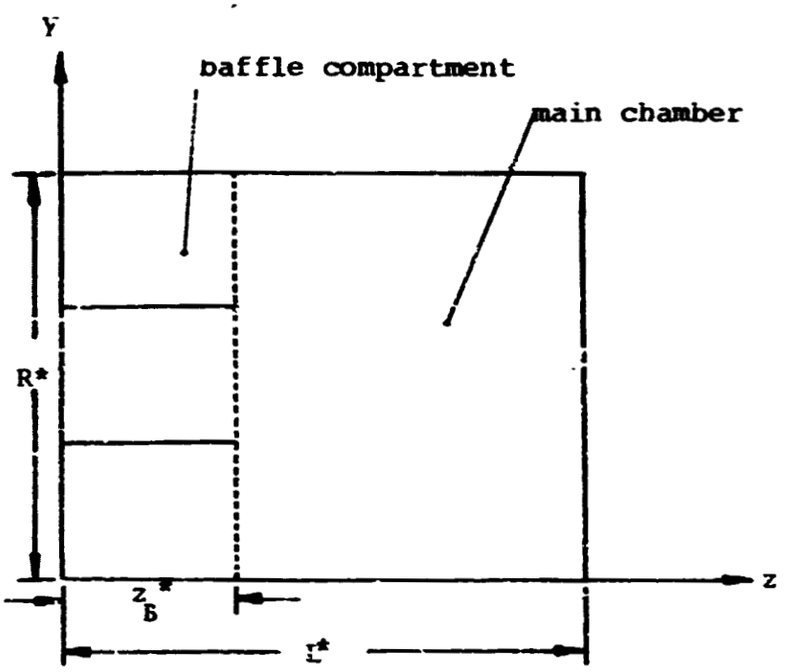

Figure 4. The two dimensional rectangular chamber.

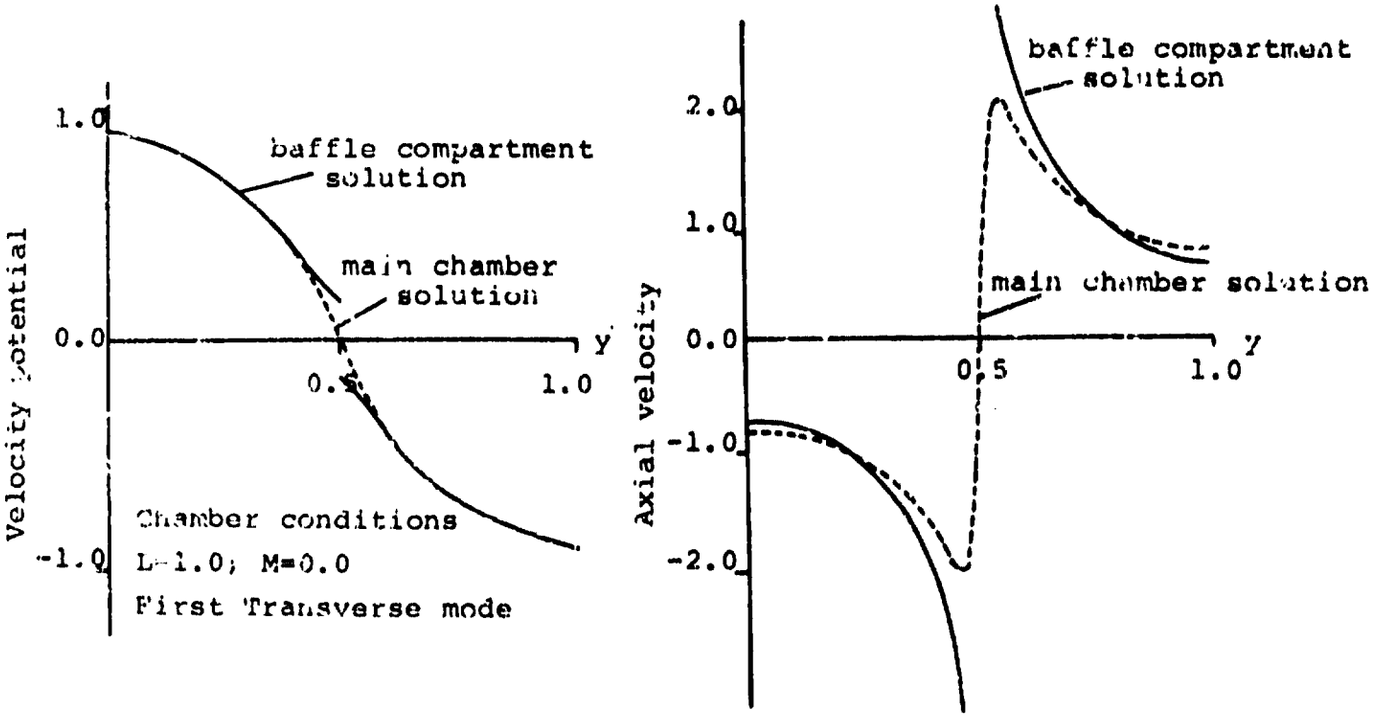

Figure 5. Axial velocity and velocity potential at the main chamber-baffle compartment interface in a chamber with a two compartment baffle with blade length z_B=0.3.

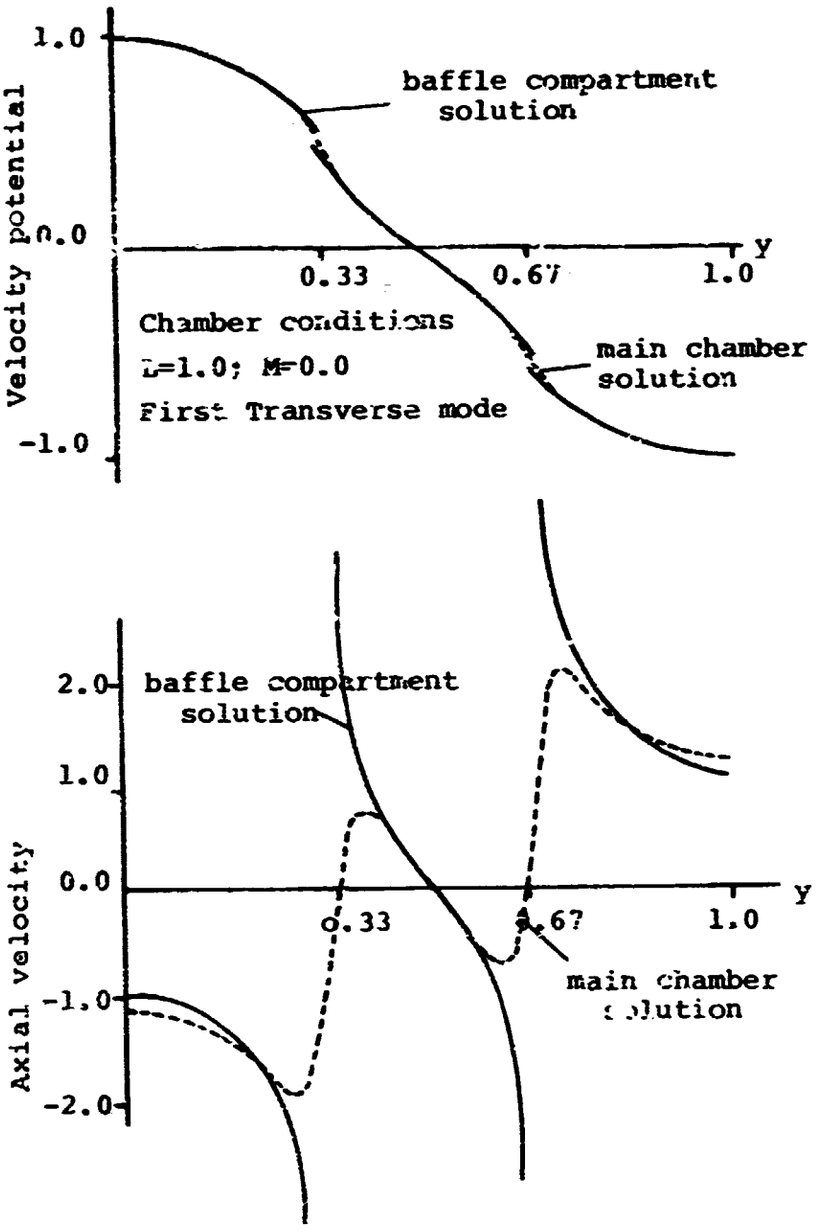

Figure 6. Axial velocity and velocity potential at the main chamber-baffle compartment interface in a chamber with a three compartment baffle with blade length z_B=0.3.

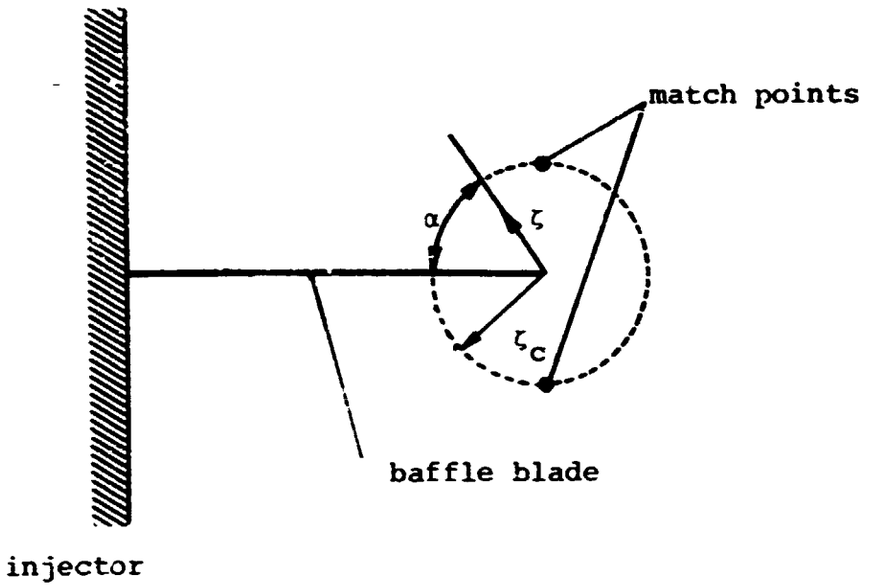

Figure 7. Polar coordinate system at baffle blade tip.

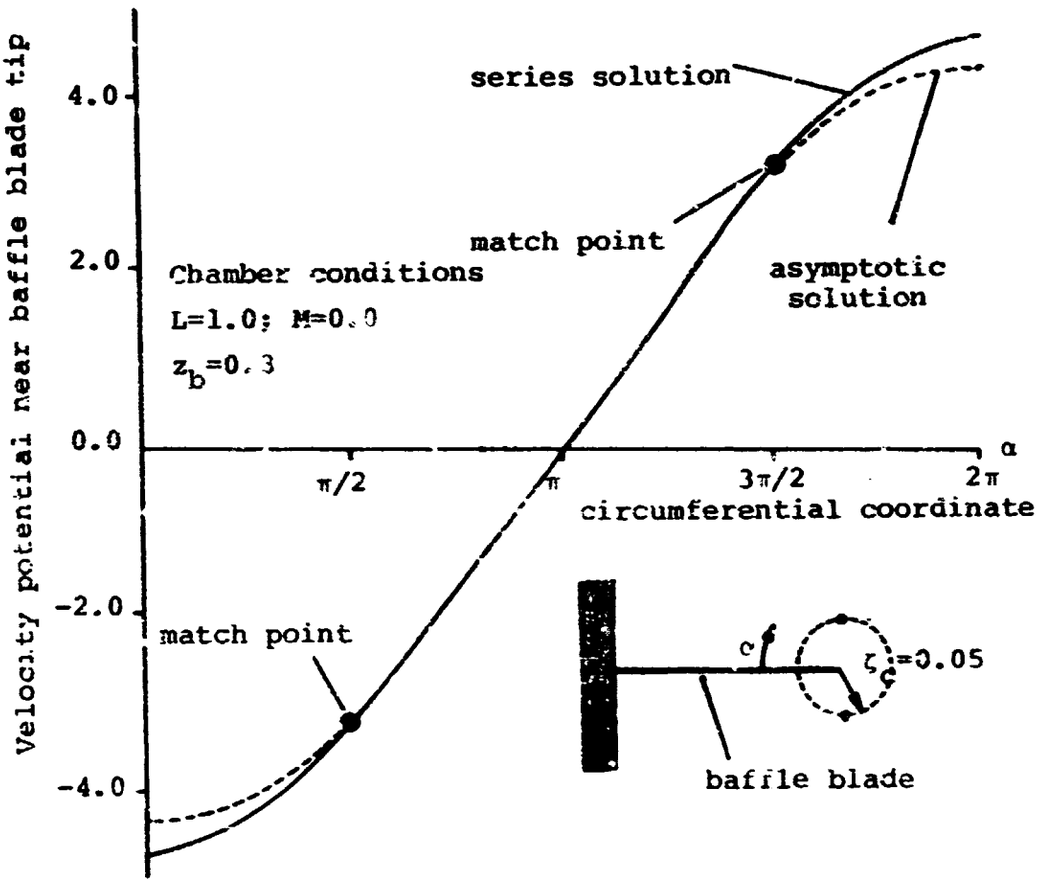

Figure 8. A comparison of the series expansion representation of the velocity potential with the asymptotic solution in a region encircling the blade tip.

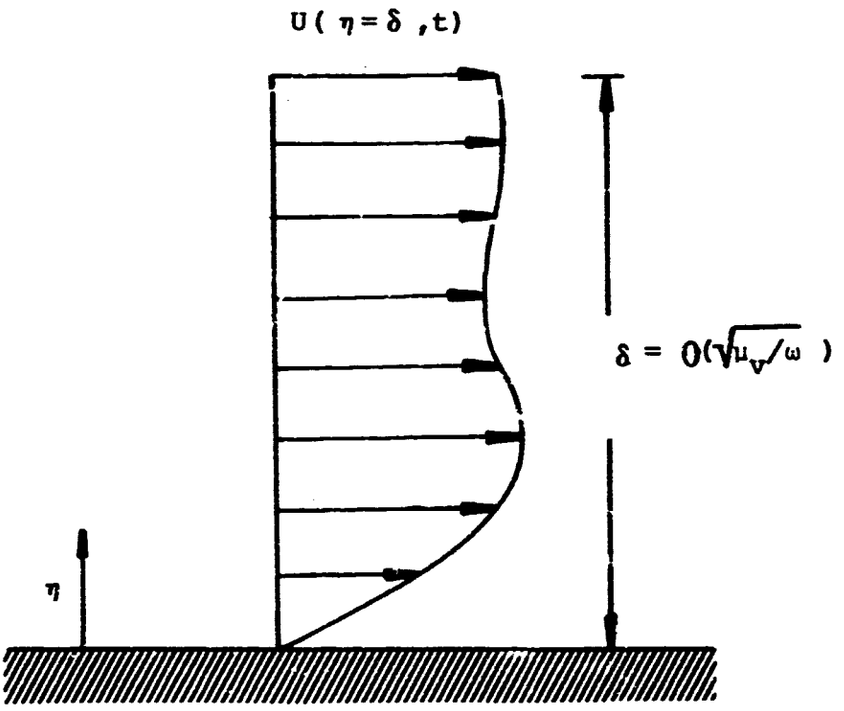

Figure 9. The geometry and notation used for the unsteady boundary layer.

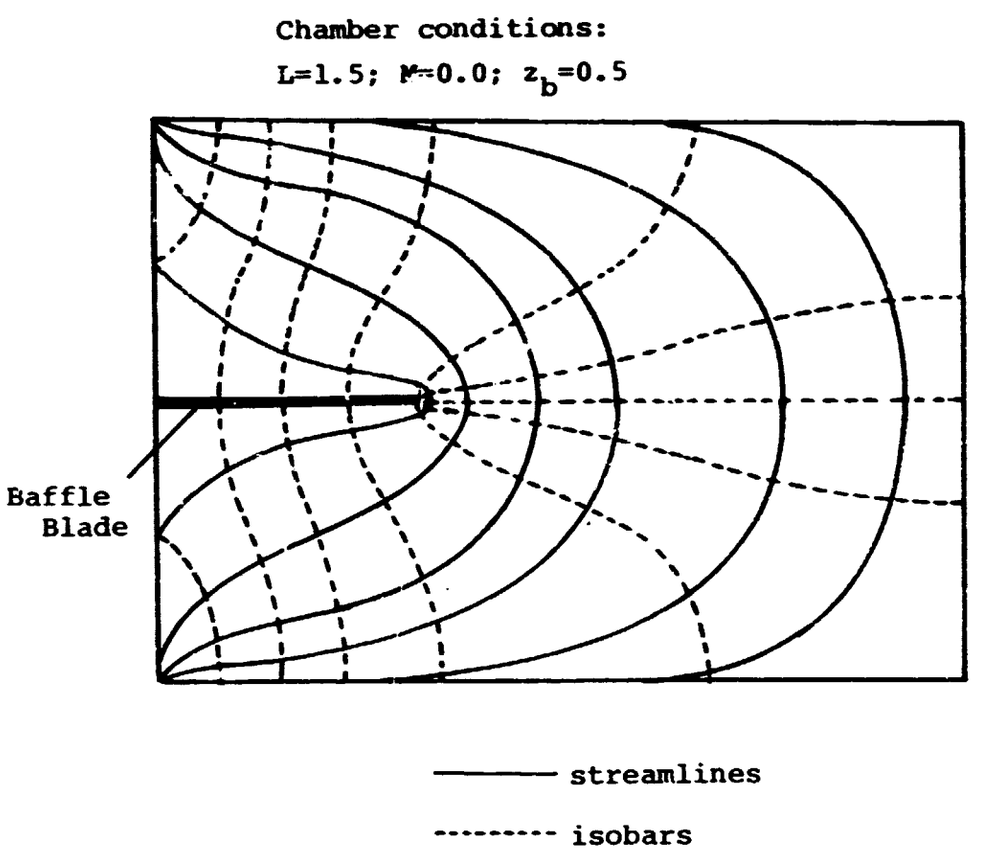

Figure 10. A streamline plot of the unsteady flow within a baffled combustor (first transverse mode in the main chamber).

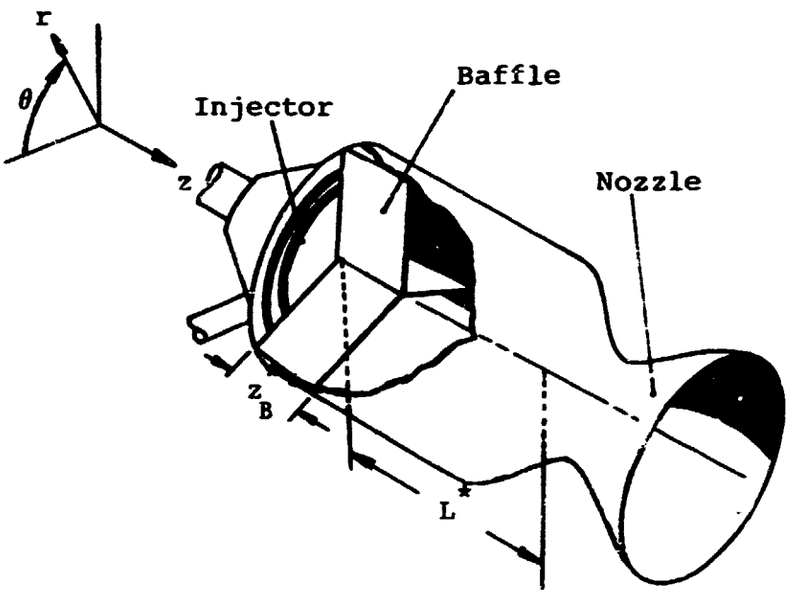

Figure 11. The geometry of the three dimensional baffled chamber.

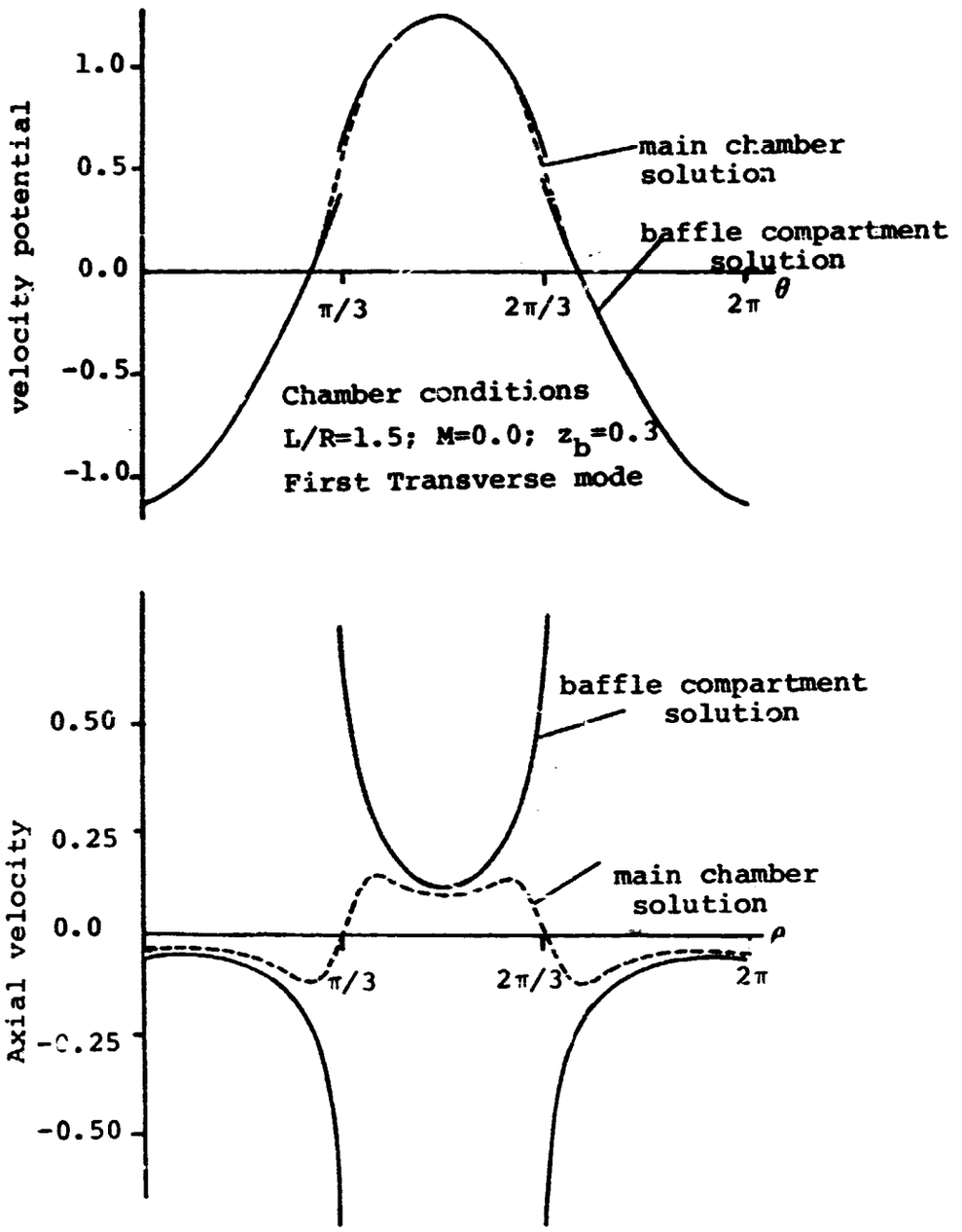

Figure 12. Axial velocity and velocity potential at the main chamber-baffle compartment interface ′and r=1.), in a cylindrical chamber with a three compartment baffle of blade length z_B=0.3.

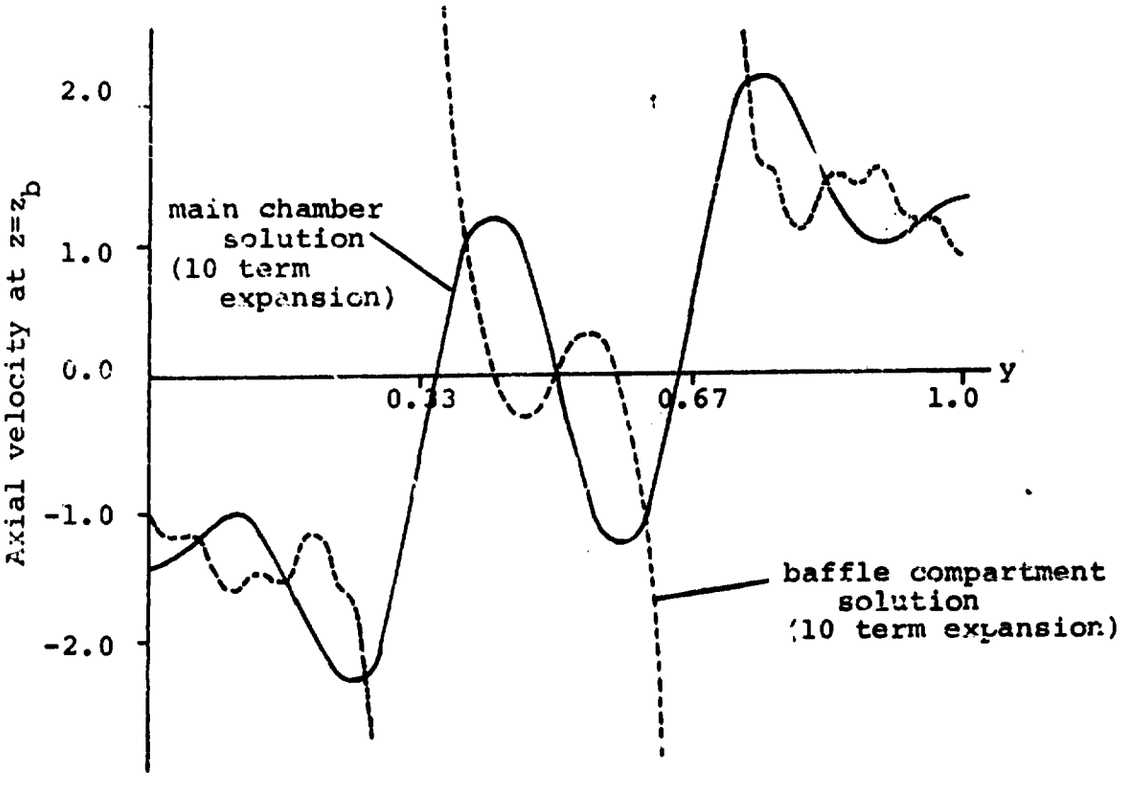

Figure 13. The comparison of the solutions of axial velocity at the main chamber-baffle compartments interface using the series expansions summed without Cesaro summation.

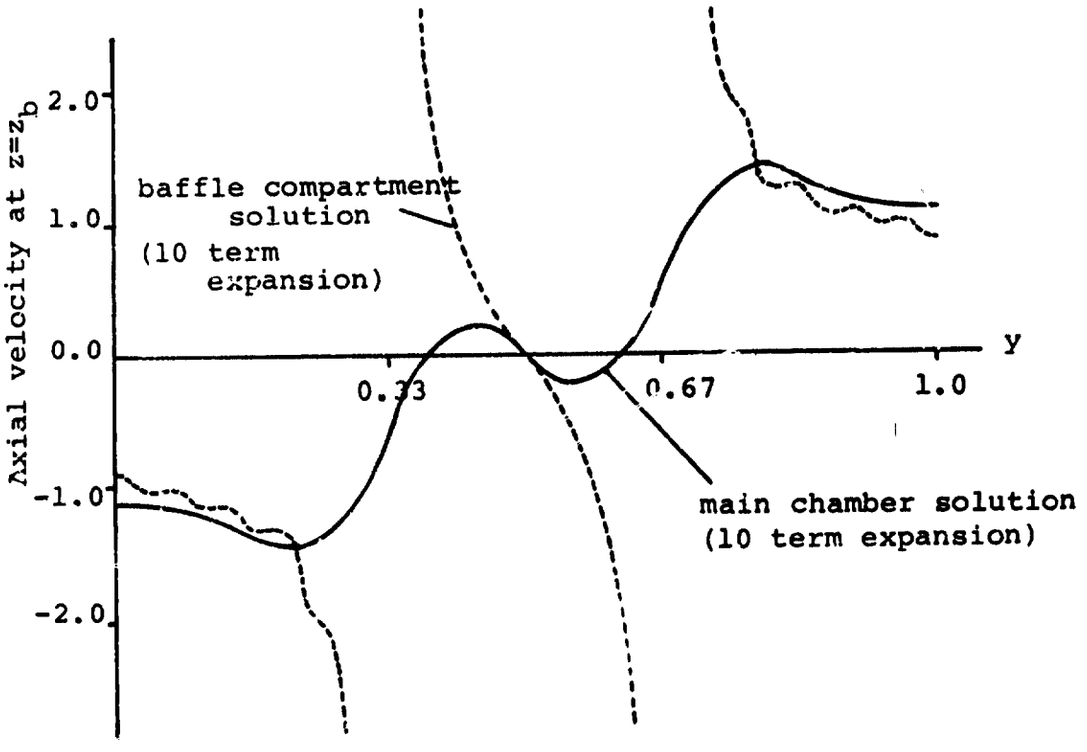

Figure 14. The comparison of the solutions of axial velocity at the main chamber-baffle compartments interface using Cesaro summation of the series expansions.

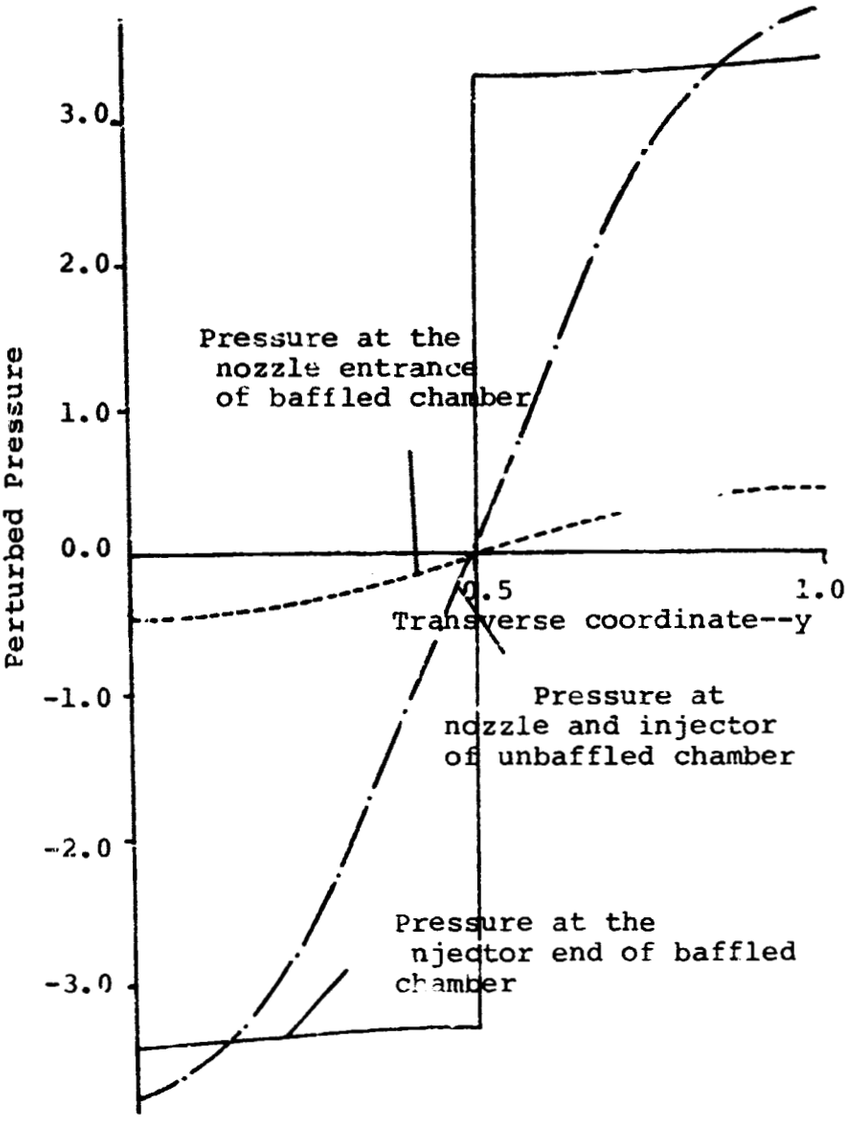

Figure 15. The profiles of the perturbed pressure at the nozzle and injector ends of a baffled and unbaffled chamber.

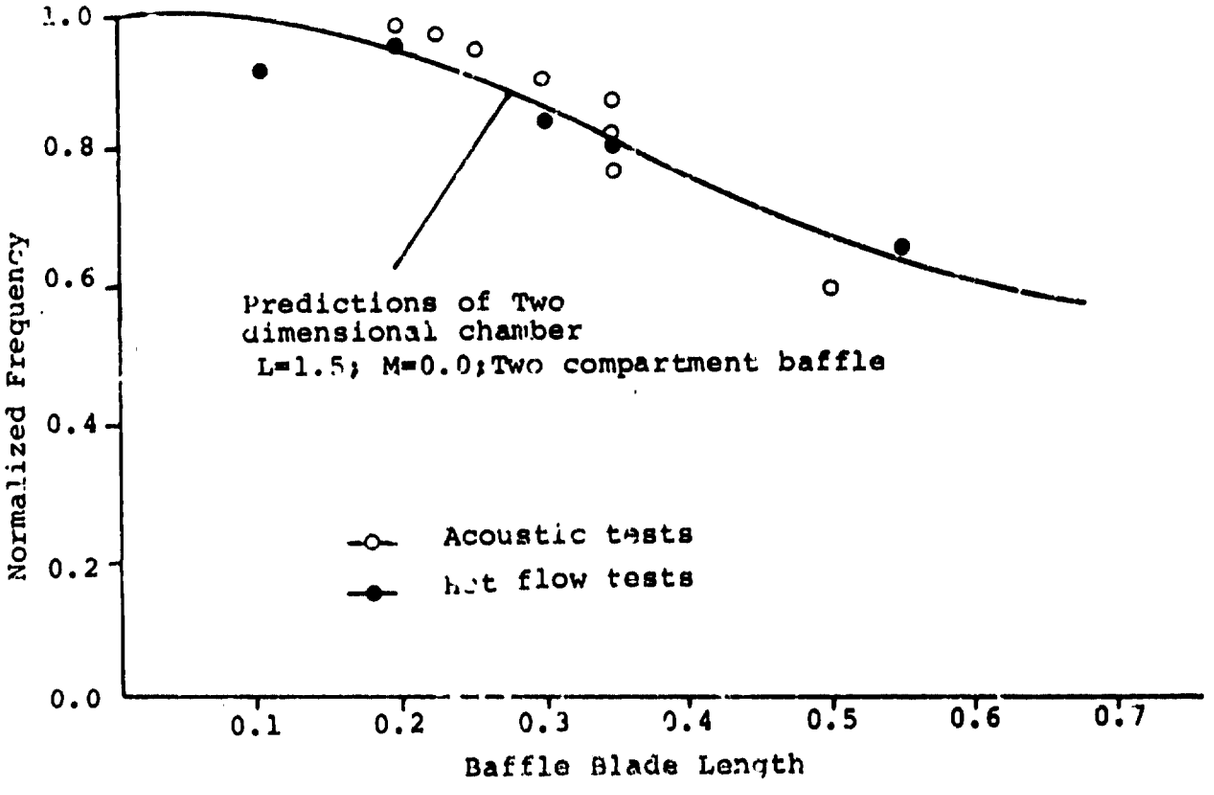

Figure 16. Prediction of the frequency depression vs. baffle blade length in a Two dimensional chamber.

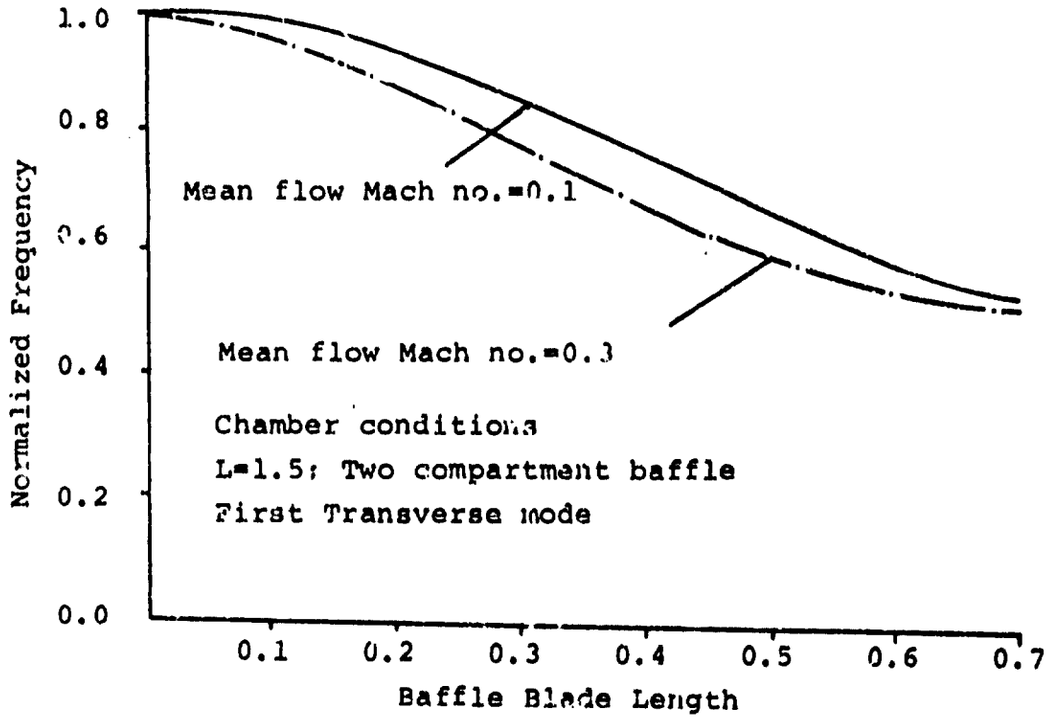

Figure 17. Mean flow Mach number corrections to the frequency vs. baffle blade length.

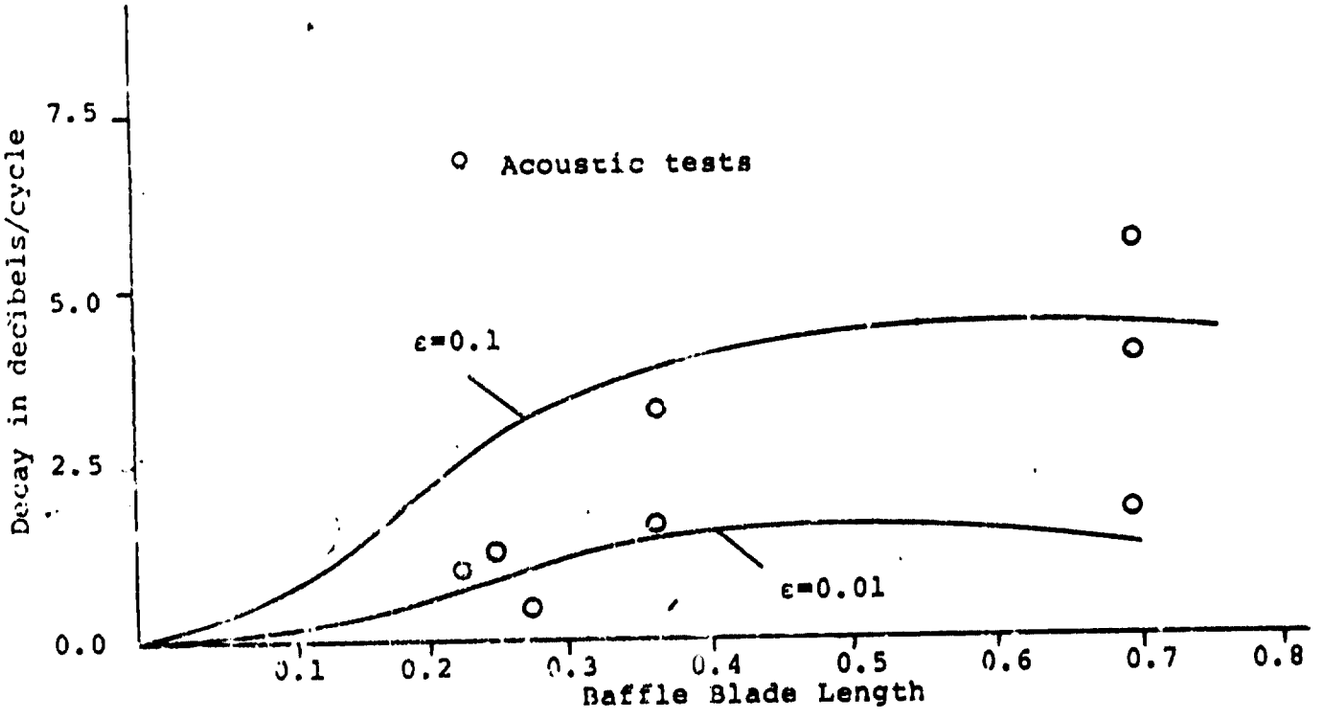

Figure 18. Decay in decibels/cycle vs. baffle blade length in a chamber which has no combustion, nozzle or mean flow effects for various wave amplitudes.

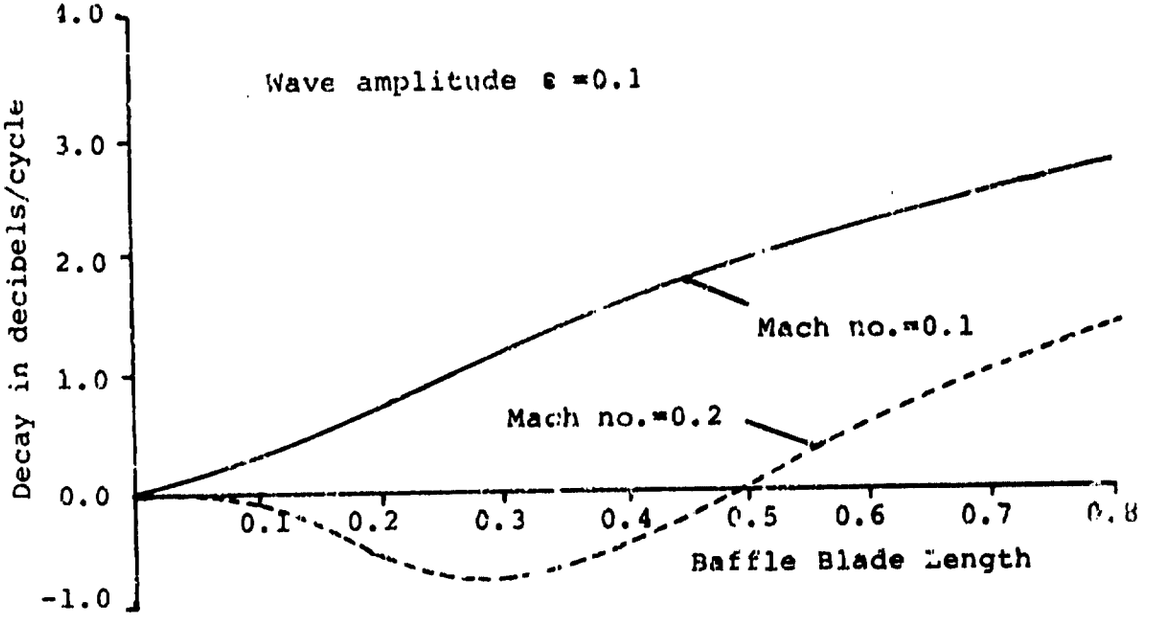

Figure 19. Mean flow, combustion and nozzle influences on the prediction of decay in decibels/cycle vs. baffle blade length.

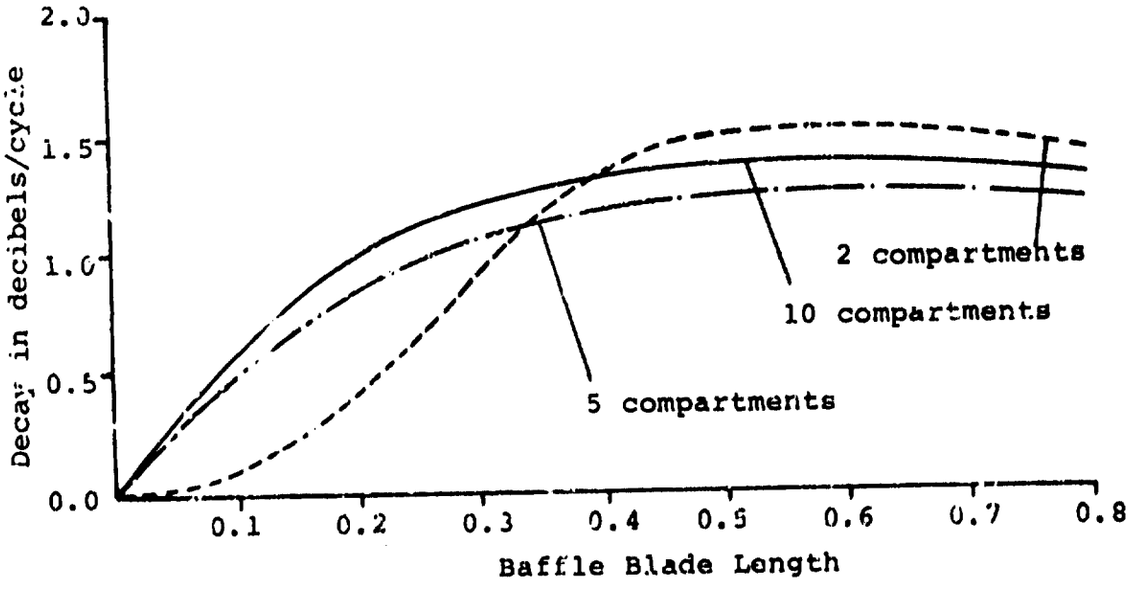

Figure 20. The effect of number of baffle compartments on the damping in decibels/cycle vs. baffle blade length.

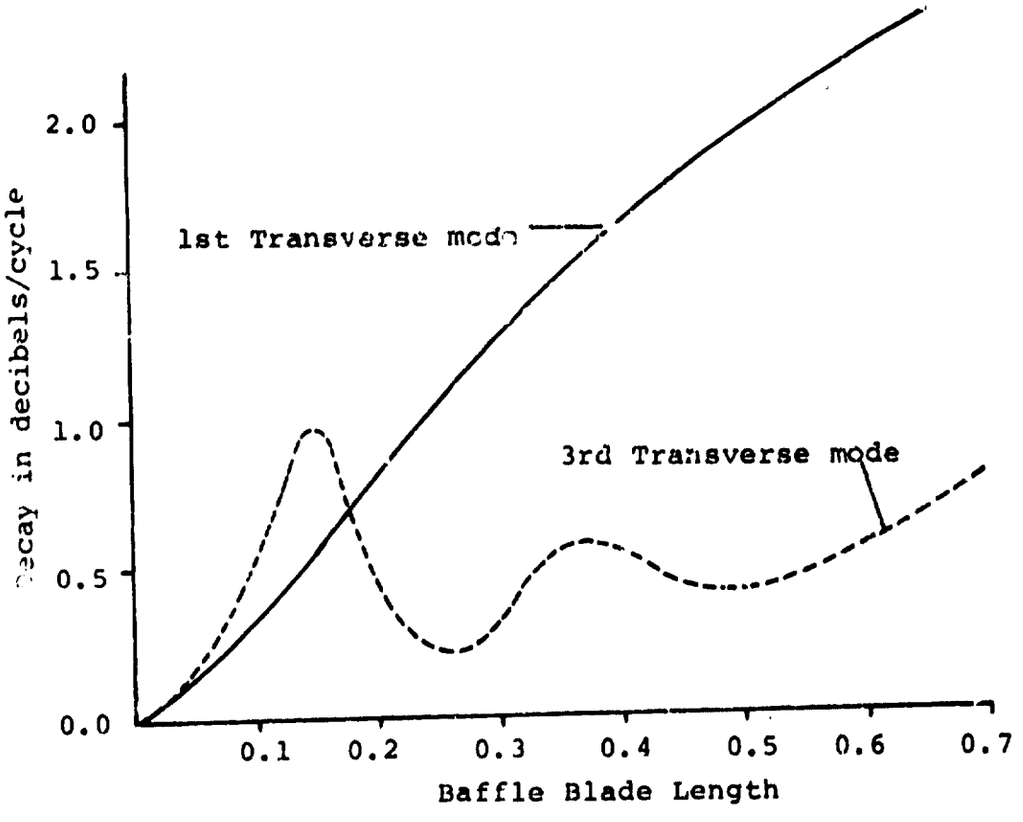

Figure 21. The predictions of damping in decibels/cycle vs. baffle blade length for various oscillation modes in the main chamber.

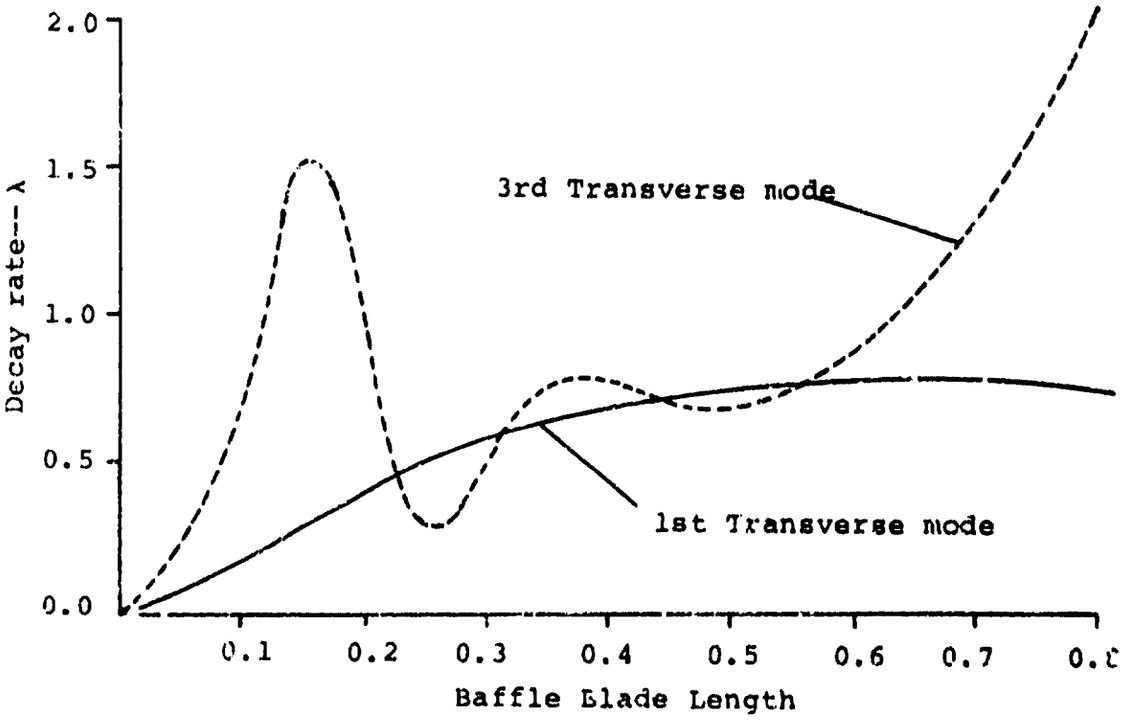

Figure 22 The decay rate (λ) vs. baffle blade length for the first and third transverse mode in the main chamber.

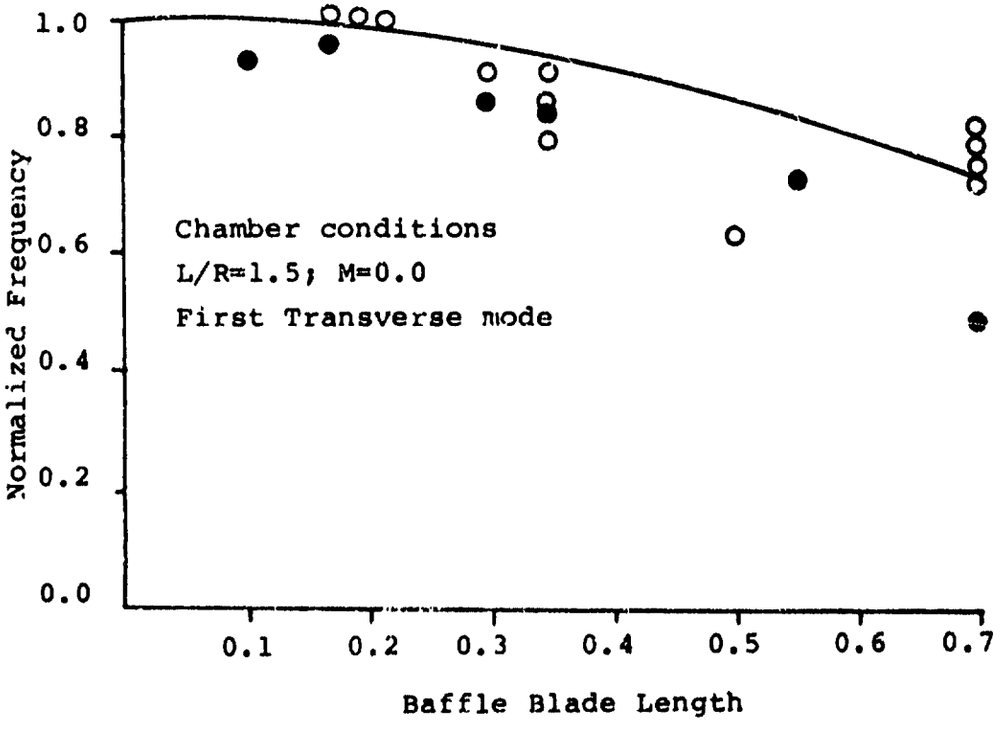

Figure 3. Normalized frequency vs. baffle blade length in a three dimensional chamber.

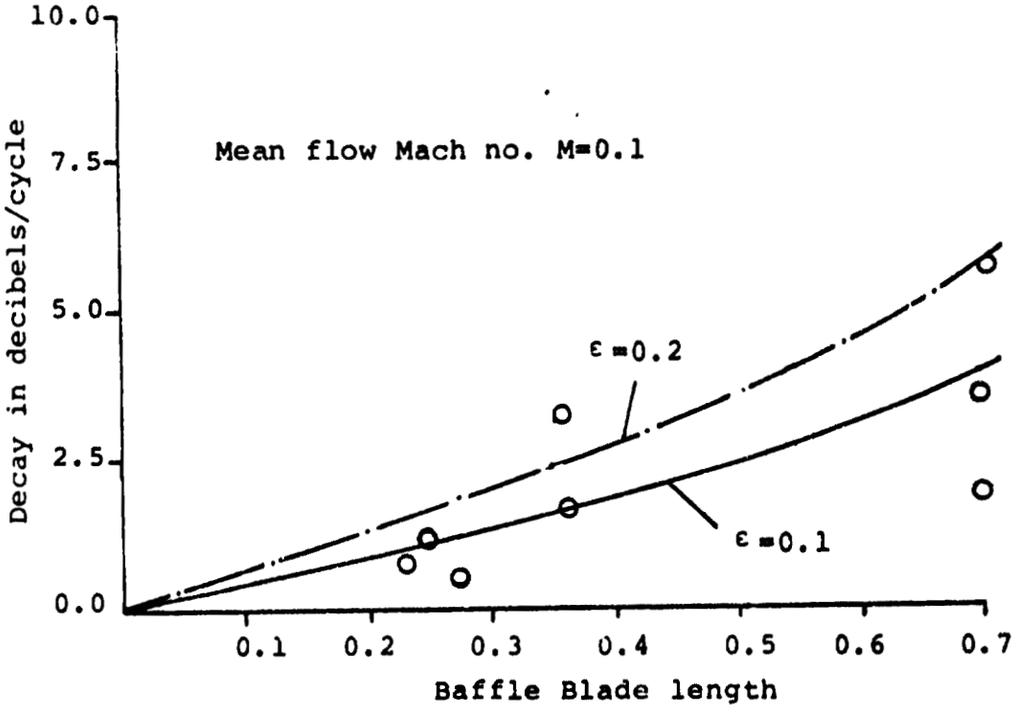

Figure 24. The effect of wave amplitude on the prediction of decay in decibels/cycle vs. baffle blade leng'

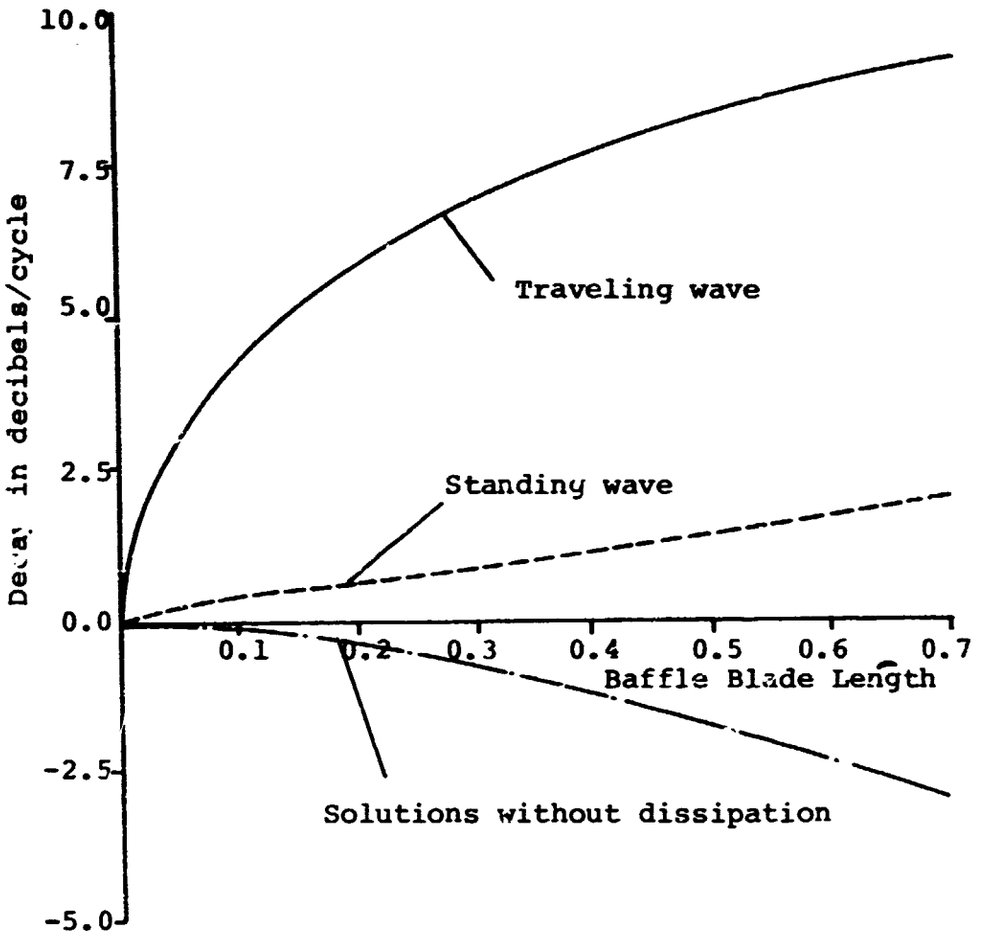

Figure 25. The standing wave and traveling wave predictions of decay in decibels/cycle vs. baffle blade length.

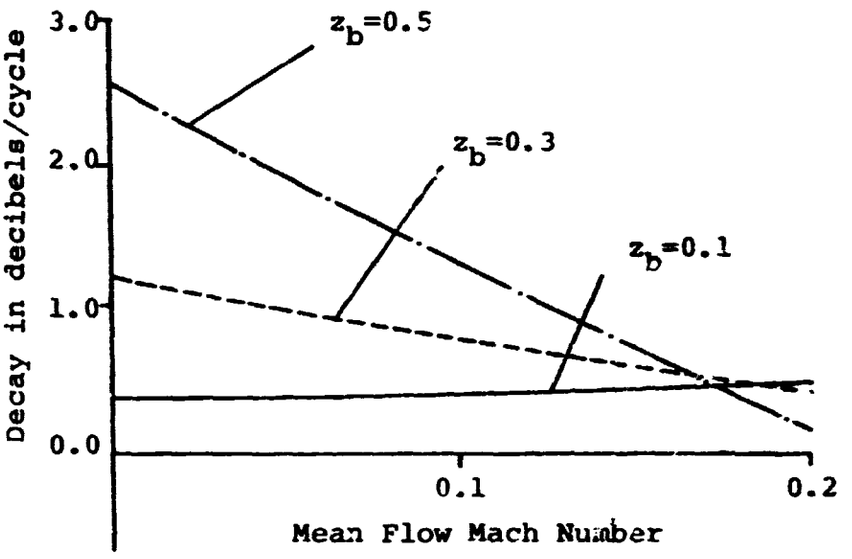

Figure 26. Mean flow Mach number corrections on decay in decibels/cycle vs baffle blade length (wave amplitude =0.1).

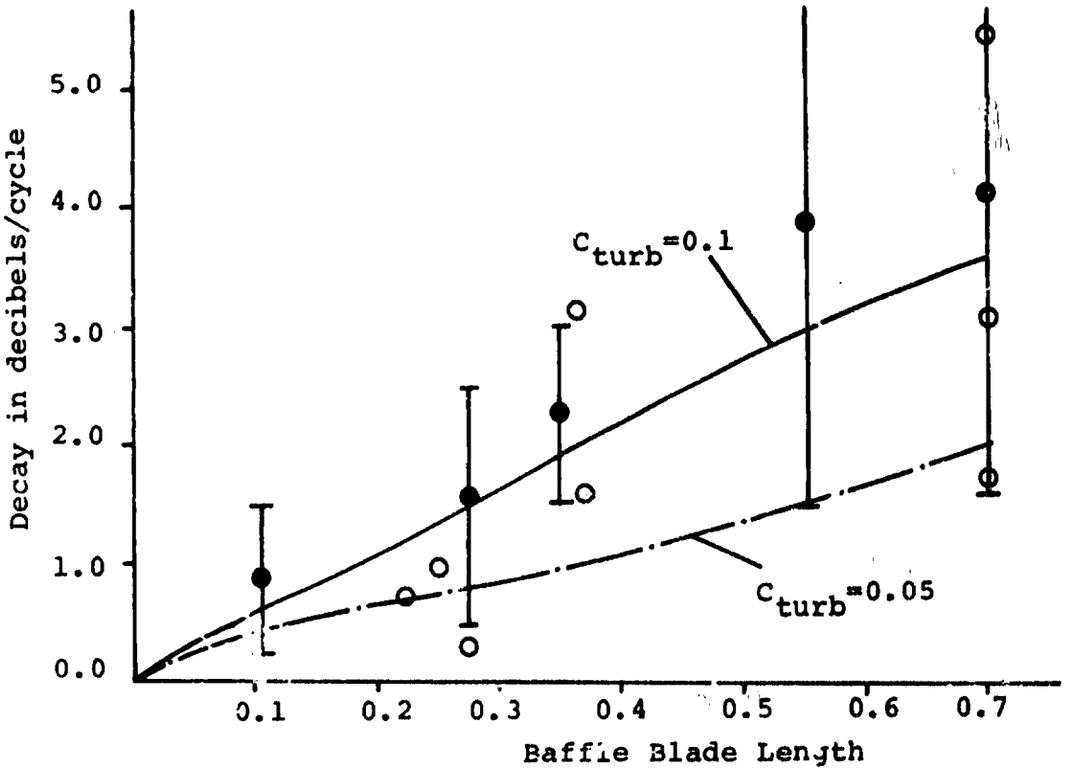

Figure 27. The effect of the turbulence coefficient (C_{turb}) on the stability predictions.

APPENDIX A

The set of constants which appear in Equation 7, 8, 19 and 20 are defined by the partial differential equation and the appropriate boundary conditions. For the two dimensional chamber these constants are defined as:

Baffle compartment - Two Dimensional Chamber

$$B_{1,B} = \frac{\omega M + \sqrt{\omega^2 M^2 + (M^2 - 1)\left((m\pi N)^2 - \omega^2\right)}}{(1 - M^2)}$$

$$B_{2,B} = \frac{\omega M - \sqrt{\omega^2 M^2 + (M^2 - 1)\left((m\pi N)^2 - \omega^2\right)}}{(1 - M^2)}$$

$$C_B = -\left[\frac{B_{1,B} + M\left[\gamma n(1 - e^{-i\omega\bar{\tau}}) - 1\right](\omega + B_{1,B})}{B_{2,B} + M\left[\gamma n(1 - e^{-i\omega\bar{\tau}}) - 1\right](\omega + B_{2,B})}\right]$$

Main Chamber - Two Dimensional Combustor

$$B_{1,c} = \frac{\omega M + \sqrt{\omega^2 M^2 + (M^2 - 1)\left((m\pi)^2 - \omega^2\right)}}{(1 - M^2)}$$

$$B_{2,c} = \frac{\omega M - \sqrt{\omega^2 M^2 + (M^2 - 1)\left((m\pi)^2 - \omega^2\right)}}{(1 - M^2)}$$

$$C_c = -\left[\frac{B_{1,c} + M(\gamma - 1)(\omega + B_{2,c})/2}{B_{2,c} + M(\gamma - 1)(\ + B_{2,c})/2}\right]$$

For the three dimensional cylindrical chamber these constants are represented as:

Baffle compartment - Three Dimensional char[illegible]

$$B_{1,B} = \frac{\omega M + \sqrt{\omega^2 M^2 + (M^2 - 1)\ (\lambda_{\ell m}^{B^2} - \omega^2)}}{(1 - M^2)}$$

$$B_{2,B} = \frac{M - \sqrt{\omega^2 M^2 + (M^2 - 1)\ (\lambda_{\ell m}^{B^2} - \omega^2}}{(1 - M^2)}$$

$$C_B = -\left[\frac{B_{1,B} + M\left[\gamma n(1 - e^{-i\omega\bar{\tau}}) - 1\right]\ (\omega + B_{1,B})}{B_{2,B} + M\left[\gamma n(1 - e^{-i\omega\bar{\tau}}) - 1\right]\ (\omega + B_{2,B})}\right]$$

Main chamber - Three Dimensional Combust[illegible]

$$B_{1,c} = \frac{\omega M + \sqrt{\omega^2 M^2 + (M^2 - 1)\ (\lambda_{\ell m}^{c^2} - \omega^2)}}{(1 - M^2)}$$

$$B_{2,c} = \frac{\omega M - \sqrt{\omega^2 M^2 + (M^2 - 1)\ (\lambda_{\ell m}^{c^2} - \omega^2)}}{(1 - M^2)}$$

$$C_c = -\left[\frac{B_{1,c} + M(\gamma - 1)\ (\omega + B_{1,c})/2}{B_{2,c} + M(\gamma - 1)\ (\omega + B_{2,c})/2}\right]$$

Appendix B

COMPUTER PROGRAMS

The computer programs used to calculate the frequency (ω) and the decay rate (λ) of oscillations for baffled combustors modeled with the influences of gain/loss end-wall boundary conditions, mean flow, and baffle tip energy dissepation are given in this section. These programs are coded in Fortran IV using complex arithematic. Two programs are written for the two-dimensional chamber (TWDB) and the three dimensional cylindrical chamber (BAFFLE). Terminating each program is a sample output.

Two Dimensional Chamber - Computer Programs TWDB

The input parameters to this program are devined as:

1. MC - Maximum number of series terms used to represent the solution in the main chamber.
2. MB - Maximum number of series terms used to represent the colution in the baffle compartments.
3. ALENGTH - Nondimensional chamber length (L^*/R^*).
4. ZB - Nondimensional baffle blade length (Z_B^*/R^*).
5. T - Nondimensional baffle blade thickness (T^*/R^*).
6. MUB - Total number of evenly spaced baffle compartments.
7. GAMMA - Ratio of specific heats.
8. EPSILON - Oscillation wave amplitude.
9. AMACH - Steady state mean flow Mach number.
10. MHAT - The transverse mode number of the dominating term in the main chamber solution.
11. IDMX - Maximum number of iterations of the successive approximation of the solution.

Other initialized parameters (not read in the program as data):

1. VISC - Nondimensional molecular viscosity ($\mu_v^*/\bar{\rho}^*\bar{a}^*R^*$).
2. CTURB - Coefficient in Spalding's effective turbulent viscosity model.
3. AM - Interaction index parameter of Crocco's time-lag model of unsteady combustion
4. TAU - Time lag of Crocco's time lag model.

The input data for program TWDB is read on three cards and has the following format:

	Columns	Variable	Type
Card 1	1-5	MC	INTEGER
	6-10	MB	INTEGER
	11-15	IDMAX	INTEGER
	16-20	MHAT	INTEGER
Card 2	1-10	ALENGTH	DECIMAL
	11-20	AMACH	DECIMAL
	21-30	GAMMA	DECIMAL
	31-40	EPSILON	DECIMAL
Card 3	1-5	MUB	INTEGER
	6-15	ZB	DECIMAL
	16-25	T	DECIMAL

A listing of the program and a sample output is contained on the following pages.

Three Dimensional Cylindrical Chamber-Program BAFFLE

The input parameters to this program are defined as:

1. MC - Maximum number of Fourier series turns in the main chamber solution.
2. LC - Maximum number of Bessel terms in the main chamber solution.
3. MB - Maximum number of Fourier terms in the baffle compartment soution.
4. LB - Maximum number of Bessel terms in the baffle compartment solution.
5. ALENGTH - Combustor length to radius ratio (L*/R*).
6. ZB - Nondimensional baffle blade length (ZB*/R*).
7. T - Nondimensional baffle blade thickness (T*/R*).
8. NUB - Number of evenly spaced baffle cavities.
9. GAMMA - Ratio of specific heats.
10. EPSILON - Oscillation wave amplitude
11. AMACH - Steady state mean flow Mach number.
12. MHAT - Dominating transverse mode of the oscillation in the main chamber.
13. LHAT - Dominating radial mode of the oscillation in the main chamber.
14. IDMAX - Maximum number of iterations of the successive approximations of the solution.

Other initialized parameters which are not input as data:

1. VISC - Molecular viscosity ($\mu_v^*/\bar{r}^*\bar{a}^*R^*$)
2. CTURB - Coefficient in Spalding's effective turbulent viscosity model.

3. AN - Interaction index.

4. TAU - Time lag

5. MX - Variable which determines the type of oscillation to be considered. MX = 0 will specify a standing wave solution and MX = 1 will yield a traveling wave solution.

The input data for program RAFFLE is read on three data cards:

	Columns	Variable	Type
Card 1	1-5	MC	INTEGER
	6-10	LC	INTEGER
	11-15	MB	INTEGER
	16-20	LB	INTEGER
	21-25	IDMAX	INTEGER
	26-30	MHAT	INTEGER
	31-35	LHAT	INTEGER
Card 2	1-10	ALENGTH	DECIMAL
	11-20	AMACH	DECIMAL
	21-30	GAMMA	DECIMAL
	31-40	EPSILON	DECIMAL
Card 3	1-5	NUB	INTEGER
	6-15	ZB	DECIMAL
	16-25	T	DECIMAL

A listing and a sample output is contained in the following pages.

```
      PROGRAM TWOD( INPUT,OUTPUT,TAPE5=INPUT,TAPE6=OUTPUT)
      COMPLEX SUMX,ANN,ALAMI,BSK,AB1,AB2,CM,EB3,SUMY,CI,BMU,
     1ALAMA,CBS,CB1,CB2,ECB1,ECB2,CCC,BSV,CCS,BB1,BB2,EB1,EB2,BCC,G1,O,
     2OMEG1,ALIN1,ALNO2,BASE,SUM2,SUM1,SUM2,VL2,VL3,AMU,A ,OMEG,BK
      DIMENSION TTE(30,30,10),BMU(30),AMU(30,10),W(11),Z(11),A(10),O(4)
      DATA(W(I),I=1,11)/.0212910183755 4,.057616658311 24,.093400398278 25,
     1.120520169614 32,.136424900956 28,.141493708928 75,.136424900956 28,
     2.120520169614 32,.093400398278 25,.057616658311 24,.021291018375 54/
      DATA(Z(I),I=1,11)/.007957319952 58,.034910077030 67,.122916636 1458,
     1.230765344947 16,.360184793419 11,.500000000000 00,.639815206550 89,
     2.769234565505 284,.877083363285 42,.953089922969 33,.992042600 4742/
C**** INPUTS INCLUDE NO. OF SERIES TERMS-MC AND MB,COMBUSTOR
C**** NONDIMENSIONAL LENGTH-ALENGTH,BAFFLE BLADE LENGTH-ZB,
C**** BAFFLE BLADE THICKNESS-T,NO. OF BAFFLE COMPARTMENTS-MUB,
C**** RATIO OF SPECIFIC HEATS-GAMMA,WAVE AMPLITUDE-EPSILON,
C**** MEAN FLOW MACH NO.-AMACH,TANSVERSE MODE CHARACTER-MMAT,
C**** AND MAXIMUM NO. OF ITERATIONS OF SUCCESSIVE APPROX. OF SERIES
      READ(5,140) MC,MB,IDMAX,MMAT
  140 FORMAT(4I5)
      READ(5,141)ALENGTH,AMACH,GAMMA,EPSILON
  141 FORMAT(4F10.5)
      READ(5,142)MUB,ZB,T
  142 FORMAT(I5,2F10.5)
      XC=XB=ZB
C**** THESE PARAMETERS ARE FOR THE DISSIPATION CALC.
      CTURB=0.034
      VISC=1.0E-05
      DISFV=SQRT(VISC)
      DISFT=SQRT(CTURB)
C**** UNSTEADY COMBUSTION INPUT PARAMETERS N AND TAU ARE DEFINED
      AN=(GAMMA+1.)/4./GAMMA
      TAU=1.
      WRITE(6,400)
      WRITE(6,400)
      WRITE(6,401)
  401 FORMAT(*0THE FOLLOWING CALC.  ARE MADE FOR A 2-D CHAMBER*)
      WRITE(6,400)
      WRITE(6,400)
  400 FORMAT(*0*, 50(1H*))
      WRITE(6,402)
  402 FORMAT(*0THE CHAMBER HAS THE FOLLOWING CONFIG.*)
      WRITE(6,403) ALENGTH,AMACH,GAMMA
  403 FORMAT(*0LENGTH=*,F10.5,3X,* MEAN FLOW MACH NO.=*,F10.5,
     13X, / ,* RATIO OF SPECIFIC HEATS=*,F10.5)
      WRITE(6,404) MUB,ZB,T
  404 FORMAT(*0THE BAFFLE CONSISTS OF *,I5,* COMPARTMENTS WITH LENGTH*,
     1F10.5,/,* AND BLADE THICKNESS*,F10.5)
      WRITE(6,405) MMAT,EPSILON
  405 FORMAT(*0THE OSCILLATION  CONSIST OF A DOMINATING*,I3,* TRANSVERSE
     1 MODE*,/,* AND IS OF WAVE AMPLITUDE*,G21.14)
      WRITE(6,337) VISC
  337 FORMAT(*0MOLECULAR VISCOSITY=*,G21.14)
      WRITE(6,407) CTURB
  407 FORMAT(*0EFFECTIVE TURBULENT VISC COEF.=*,G21.14)
      WRITE(6,408)
  408 FORMAT(*0THE FREQUENCY ITERATIONS ARE AS FOLLOWS*)
      DO 100 MU=1,MUB
      OR=MU
      OR2=MUB
      V1=OR/OR2
      V2=(OR-1.)/OR2
```

```
      DO 100 MSTAR=1,MB
      DO 100 M=1,MC
      B1=3.14159265359*((MSTAR-1.)*MUB-(M-1.))
      BO=B1*E1
      IF(BO.LT.1.0E-06) GOTO 101
      B2=3.14159265359*((MSTAR-1.)*MUB+(M-1.))
      BAS1=(SIN(B1*V1)-SIN(B1*V2))/(2.*B1)
      BAS2=(SIN(B2*V1)-SIN(B2*V2))/(2.*B2)
      TTE(MSTAR,M,MU)=BAS1+BAS2
      GOTO 100
  101 EP=1.
      IF(M.EQ.1) EP=2.
      TTE(MSTAR,M,MU)=EP/(2.*MUB)
  100 CONTINUE
  999 CONTINUE
  560 CONTINUE
C**** FIRST GUESS OF FREQUENCY
      OMEG=MMAT*(3.14159265359-2.*TB)
      DO 300 M=1,MC
  300 BMU(M)=CMPLX(0.0,0.0)
      BMU(MMAT+1)=CMPLX(1.0,0.0)
      PI=3.14159265359
      CI=CMPLX(0.0,1.0)
      MS=MMAT+1
      Q(1)=CMPLX(1.0,0.0)
      Q(2)=CMPLX(0.0,1.0)
      Q(3)=CMPLX(-1.0,0.0)
      Q(4)=CMPLX(0.0,-1.0)
      ID=0
   85 CONTINUE
      DEL=0.1
      SUMX=CMPLX(0.0,0.0)
      ANN=AN*(1.-CEXP(-CI*OMEG*TAU))-1./GAMMA
      ALAMI=-GAMMA*CI*OMEG*AMACH*ANN/(1.-GAMMA*AMACH*AMACH*ANN)
      EPM=1.
      IF(MMAT.EQ.0) EPM=2.
      IF(ID.EQ.0) GOTO 500
      EPS=2.
      DO 502 MST=1,MS
      OR=(MST-1.)*MUB
      BSK=OMEG*OMEG*AMACH*AMACH*(AMACH*AMACH-1.)*(OR*OR-OMEG*OMEG)
      BSK=CSQRT(BSK)
      AB1=(OMEG*AMACH+BSK)/(1.-AMACH*AMACH)
      AB2=(OMEG*AMACH-BSK)/(1.-AMACH*AMACH)
      CM=-(CI*AB1-ALAMI)/(CI*AB2-ALAMI)
      EB1=CEXP(CI*AB1*ZB)
      EB2=CEXP(CI*AB2*ZB)
      EB3=CI*(AB1*EB1+CM*AB2*EB2)/(EB1+CM*EB2)
      SUMY=CMPLX(0.0,0.0)
      DO 503 M=1,MC
      IF(M.EQ.MS) GOTO 503
      TUM=0.0
      DO 504 MU=1,MUB
  504 TUM=TUM+TTE(MST,MS,MU)*TTE(MST,M,MU)
      SUMY=SUMY+BMU(M)*TUM
  503 CONTINUE
      SUMX=SUMX+4.*MUB*EB3*SUMY/EPM/EPS
  502 EPS=1.
  500 CONTINUE
  223 IN=0
  215 CONTINUE
```

```
      ANN=AN*(1.-CEXP(-CI*OMEG*TAU))-1./GAMMA
      ALAMI=-GAMMA*CI*OMEG*AMACH*ANN/(1.+GAMMA*AMACH*AMACH*ANN)
      AB=AMACH*(GAMMA-1.)/2.
      ALAMN=-CI*OMEG*AB/(1.+AMACH*AB)
      CBS=CSQRT(OMEG*OMEG-AMACH*AMACH*(AMACH*AMACH-1.)*(XHAT*XHAT*PI*PI-
     1OMEG*OMEG))
      CB1=(OMEG*AMACH*CBS)/(1.-AMACH*AMACH)
      CB2=(OMEG*AMACH-CBS)/(1.-AMACH*AMACH)
      ECB1=CEXP(CI*CB1*(ZB-ALENGTH))
      ECB2=CEXP(CI*CB2*(ZB-ALENGTH))
      CCC=-(CI*CB1-ALAMI)/(CI*CB2-ALAMN)
      BSV=CI*(CB1*ECB1-CB2*CCC*ECB2)/(ECB1-CCC*ECB2)
      SUMY=CMPLX(0.0,0.0)
      EPS=2.
      DO 55) M=1,MB
      OR=(M-1.)*PI*MUB
      CCS=CSQRT(OMEG*OMEG*AMACH*AMACH*(AMACH*AMACH-1.)*(OR*OR-OMEG*OMEG)
     1)
      BB1=(OMEG*AMACH*CCS)/(1.-AMACH*AMACH)
      BB2=(OMEG*AMACH-CCS)/(1.-AMACH*AMACH)
      EB1=CEXP(CI*BB1*ZB)
      EB2=CEXP(CI*BB2*ZB)
      BCC=-(CI*BB1-ALAMI)/(CI*BB2-ALAMI)
      TUM=0.0
      DO 551 MU=1,MUB
  551 TUM=TUM+(TTE(M,MS,MU))**2
      SUMY=SUMY+4.*MUB*TUM*CI*(BB1*EB1-BB2*BCC*EB2)/EPS/EPM/(EB1-BCC*EB2
     1)
  550 EPS=1.
      G1=BSV-SUMY-SUMX
      G=CABS(G1)
      IF(IN.NE.0) GOTO 224
  223 OMEG1=OMEG
      REF=G
      IN=1
      GOTO 225
  224 IF(G.LT.REF) GOTO 223
      IF(IN.LT.4) GOTO 228
      OMEG=OMEG1
      DEL=DEL/2.
      IF(DEL.LT.1.E-03) GOTO 310
      IN=1
      GOTO 225
  228 IN=IN+1
  225 OMEG=OMEG1-G(IN)*DEL
      GOTO 215
  310 CONTINUE
      ID=ID+1.
      WRITE(6,410) ID,OMEG
  410 FORMAT(*0ITERATION *,I3,* COMPLEX FREQ.=*,2G21.14)
      IF(ID.GT.IDMAX) GOTO 900
C**** ITERATION OF MAIN CHAMBER SERIES COEF.
      ALINJ=ALAMI
      ALNOZ=ALAMN
      EPP=2.
      DO 200 MP=1,MC
      IF(MP.EQ.MS) GOTO 200
      OR=(MP-1.)*PI
      BASE=OMEG*OMEG*AMACH*AMACH-(AMACH*AMACH-1.)*(OR*OR-OMEG*OMEG)
      BASE=CSQRT(BASE)
      CB1=(OMEG*AMACH+BASE)/(1.-AMACH*AMACH)
```

```
      CB2=(OMEG*AMACH-BASE)/(1.-AMACH*AMACH)
      CCC=-(CI*CB1-ALNOZ)/(CI*CB2-ALNOZ)
      ECB1=CEXP(CI*CB1*(ZB-ALENGTH))
      ECB2=CEXP(CI*CB2*(ZB-ALENGTH))
      CBS=CI*(CB1*ECB1+CB2*CCC*ECB2)/(ECB1+CCC*ECB2)
      SUMY=CMPLX(0.0,0.0)
      SUMX=CMPLX(0.0,0.0)
      EPS=2.
      DO 201 MST=1,MB
      OR=(MST-1.)*PI*MUB
      BASE=CSQRT(OMEG*OMEG*AMACH*AMACH+(AMACH*AMACH-1.)*(OR*OR-OMEG*OMEG
     1))
      BB1=(OMEG*AMACH+BASE)/(1.-AMACH*AMACH)
      BB2=(OMEG*AMACH-BASE)/(1.-AMACH*AMACH)
      BCC=-(CI*BB1-ALINJ)/(CI*BB2-ALINJ)
      EB1=CEXP(CI*BB1*ZB)
      EB2=CEXP(CI*BB2*ZB)
      TUM=0.0
      DO 202 MU=1,MUB
  202 TUM=TUM+(TTE(MST,MP,MU))**2
      BASE=CI*(BB1*EB1+BB2*BCC*EB2)/(EB1+BCC*EB2)
      SUMX=SUMX+4.*MUB*BASE*TUM/EPS/EPP/CBS
      SUMZ=CMPLX(0.0,0.0)
      DO 203 M=1,MC
      IF(M.EQ.MP) GOTO 203
      TUM=0.0
      DO 204 MU=1,MUB
  204 TUM=TUM+TTE(MST,MP,MU)*TTE(MST,M,MU)
      SUMZ=SUMZ+BMU(M)*TUM
  203 CONTINUE
      SUMY=SUMY+SUMZ*4.*MUB*BASE/EPS/EPP/CBS
  201 EPS=1.
      BMU(MP)=SUMY/(1.-SUMX)
  200 EPP=1.
      GOTO 85
  900 CONTINUE
      WRITE(6,915)
  915 FORMAT(*0THE MATRIX OF THE MAIN CHAMBER FOURIER COEF.=*)
      DO 911 M=1,MC
      WRITE(6,910)M,BMU(M)
  910 FORMAT(* *,I3,* *,2G21.14)
  911 CONTINUE
      DO 901 MU=1,MUB
      DO 901 M=1,MB
      SUMX=CMPLX(0.0,0.0)
      DO 902 MP=1,MC
  902 SUMX=SUMX+BMU(MP)*TTE(M,MP,MU)
      EP=1.
      IF(M.EQ.1) EP=2.
      BASEX=EP/(2.*MUB)
      OR=MB-M+1.
      OR1=MB
      SUMX=SUMX*OR/OR1
  901 AMU(M,MU)=SUMX/BASEX
      DO 913 MU=1,MUB
      WRITE(6,914) MU
      DO 912 M=1,MB
  912 WRITE(6,910)M,AMU(M,MU)
  913 CONTINUE
  914 FORMAT(*0THE MATRIX OF FOURIER COEF. FOR THE BAFFLE COMP.*,I3)
  985 CONTINUE
```

```
      MUBX=MUB-1
      DO 778 MU=1,MUBX
      SUM1=SUM2=CMPLX(0.0,0.0)
      Y1=MU/MUB-T
      Y2=MU/MUB+T
      DO 779 M=1,M6
      VL1=(M-1.)*PI*MUB
      VL2=AML(M,MU)*COS(VL1*Y1)
      VL3=AML(M,MU+1)*COS(VL1*Y2)
      SUM1=SUM1+VL2
  779 SUM2=SUM2+VL3
      A(MU)=(SUM2-SUM1)/SQRT(2.*T)
  778 CONTINUE
C**** DISSIPATION CALCULATION
      OM=REAL(OMEG)
      AMULT=GAMMA*SQRT(OM  /2.)/2.
      SUM=0.0
      TE=ACOS(ZB/(ZB+T))
      DO 339 MU=1,MUBX
      ABX=CABS(A(MU))
      ABX=ABX*ABX
      B=EPSILON*EPSILON*ABX*T/4.
      SUM1=0.0
      DO 336 I=1,11
      ETA=TE/2.+Z(I)*(PI-TE)/2.
      V1=SIN(ETA)
  336 SUM1=SUM1+(DISFV+DISFT*((AMACH*AMACH+B*V1*V1)**0.25))*W(I)/V1
      SUM1=ABX*SUM1*(PI-TE)/2.
  339 SUM=SUM+SUM1
      SUM=AMULT*SUM
      OMG=REAL(OMEG)
C**** DECAY RATE CALCULATION
      BINI=0.0
      SUMY1=0.0
      EPM=2.
      DO 821 M=1,M4
      OR=PI*(M-1.)*MUB
      BSK=CSQR((OMEG*OMEG*AMACH*AMACH*(AMACH*AMACH-1.)*(OR*OR-OMEG*OMEG)
     1))
      AB1=(OMEG*AMACH*BSK)/(1.-AMACH*AMACH)
      AB2=(OMEG*AMACH-BSK)/(1.-AMACH*AMACH)
      CM=-(CI*AB1-ALAM1)/(CI*AB2-ALAM1)
      BASE=CEXP(CI*AB1*ZB)+CM*CEXP(CI*AB2*ZB)
      BAS=CABS(BASE)
      BAS=BAS*BAS
      BB1=(1.+CM)*CI*OMEG*AMACH*CI*(AB1+AB2*CM)
      BASR=CABS(BB1)
      BASR=BASR*BASR*GAMMA*GAMMA
      SUMW1=0.0
      DO 822 I=1,11
      ETA=ZB*Z(I)
      BSK=CEXP(CI*AB1*ETA)+CM*CEXP(CI*AB2*ETA)
      BS1=CABS(BSK)
      BB2=CI*(BSK*CEXP(CI*AB1*ETA)+CM*AB2*CEXP(CI*AB2*ETA))
      BSR=GAMMA*(CI*OMEG*BSK-AMACH*BB2)
      BS =CABS(BSK)
      BS=BS*BS/2./GAMMA/GAMMA/OMG/OM *BS1*BS1/2.
  822 SUMW1=SUMW1+BS*W(I)*ZB/2.
      RAM=0.0
      DO 823 ML=1,MUB
      RAM1=CABS(AMU(M,MU))
```

```
823 RAM=RAM*RAM1*RAM1
    BINI=BINI+RAM*BASR*EPM/BAS/FLOAT(MUB)/2.
    SUMY1=SUMY1+RAM*EPM*SUMW1/FLOAT(MUB)/2.
821 EPM=1.
    BNZI=0.0
    SUMU1=0.0
    EPM=2.
    DO 841 M=1,MC
    OR=PI*(M-1.)
    BK=CSQRT(OMEG*OMEG*AMACH*AMACH+(AMACH*AMACH-1.)*(OR*OR-OMEG*OMEG))
    CB1=(OMEG*AMACH+BK)/(1.-AMACH*AMACH)
    CB2=(OMEG*AMACH-BK)/(1.-AMACH*AMACH)
    CM=-(CI*CB1-ALAMN)/(CI*CB2-ALAMN)
    BASE=CEXP(CI*CB1*(ZB-ALENGTH))+CM*CEXP(CI*CB2*(ZB-ALENGTH))
    BAS=CABS(BASE)
    BAS=BAS*BAS
    BB1=(1.+CM)*CI*OMEG+AMACH*CI*(CB1+CM*CB2)
    BASR=CABS(BB1)
    BASR=BASR*BASR*GAMMA*GAMMA
    SUMV1=0.0
    DO 842 I=1,11
    ETA=ZB+(ALENGTH-ZB)*Z(I)
    BSK=CEXP(CI*CB1*(ETA-ALENGTH))+CM*CEXP(CI*CB2*(ETA-ALENGTH))
    BS1=CABS(BSK)
    BB2=CI*(CB1*CEXP(CI*CB1*(ETA-ALENGTH))+CM*CB2*CEXP(CI*CB2*(
   1ETA-ALENGTH)))
    BSK=GAMMA*(CI*OMEG*BSK+AMACH*BB2)
    ANZB=AMACH*(1.+GAMMA)/2./GAMMA
    BS =CABS(BSK)
    BS=BS*BS/2./GAMMA+GAMMA*OMG*OMG*BS1*BS1/2.
842 SUMV1=SUMV1+BS*W(I)*(ALENGTH-ZB)/BAS
    RAM1=CABS(BMU(M))
    BNZI=BNZI+RAM1*RAM1*BASR*EPM/BAS/2.
    SUMU1=SUMU1+RAM1*RAM1*SUMV1*EPM/2.
841 EPM=1.
    BINIR=BINI/2.
    BNZIR=BNZI/2.
    EN=AN*(1.-COS(OMG*TAU))*AMACH
    BINIR=EN*BINIR
    BNZIR=ANZB*BNZIR
    SUMIN=BNZIR-BINIR+SUM
    WRITE(6,30) BINIR,BNZIR,SUM
 30 FORMAT('0COMB. INPUT',G13.6,' NOZZLE EXT.=',G13.6,' DISS.=',G13.6
   1)
    SUMY1=SUMU1+SUMY1
    DECYRT=SUMIN/SUMY1
    WRITE(6,125) DECYRT
125 FORMAT('0DECAY RATE=',G21.14)
    DECTB=54.575*DECYRT/OMEG
    WRITE(6,130) DECTB
130 FORMAT('0DECAY IN DECIBELS /CYCLE=',G21.14)
    END
```

```
**************************************************

**************************************************

THE FOLLOWING CALC.  ARE MADE FOR A 2-D CHAMBER

**************************************************

**************************************************

THE CHAMBER HAS THE FOLLOWING CONFIG.

LENGTH=    1.50000     MEAN FLOW MACH NO.=      .10000
RATIO OF SPECIFIC HEATS=    1.20000

THE BAFFLE CONSISTS OF      2 COMPARTMENTS WITH LENGTH     .50000
AND BLADE THICKNESS     .05000

THE OSCILLATION  CONSIST OF A DOMINATING  1 TRANSVERSE MODE
AND IS OF WAVE AMPLITUDE  .10000000000000

MOLECULAR VISCOSITY= 1.00000000000000E-05

EFFECTIVE TURBULENT VISC COEF.= 3.40000000000000E-02

THE FREQUENCY ITERATIONS ARE AS FOLLOWS

ITERATION    1 COMPLEX FREQ.=  2.2150301535900      -.10000000000000

ITERATION    2 COMPLEX FREQ.=  2.1322176535899     -9.687499999999998E-02

ITERATION    3 COMPLEX FREQ.=  2.1322176535899     -9.531249999999995E-02

ITERATION    4 COMPLEX FREQ.=  2.1322176535899     -9.531249999999995E-02

ITERATION    5 COMPLEX FREQ.=  2.1322176535899     -9.531249999999995E-02

ITERATION    6 COMPLEX FREQ.=  2.1322176535899     -9.531249999999995E-02

THE MATRIX OF THE MAIN CHAMBER FOURIER COEF.=
  1 -4.181518526001688E-13-6.780446697729596E-13
  2   1.000000000000000      0.
  3 -1.763831965088536E-13 2.074276168937626E-15
  4  -.1439945607002626     -2.433194388376036E-03
  5  1.542157579509426E-13 2.405577245746566E-15
  6  6.476527008655236E-02 9.813939016847866E-04
  7 -1.637884506442146E-14 1.865172049753746E-16
  8 -3.844278100137486E-02-5.443426026394556E-04
  9  1.049699766000668E-13 1.189558653698896E-15
 10  2.604813010365686E-02 3.527844379939216E-04
 11  1.034999542891286E-14 2.623596119959576E-17
 12 -1.908701755168316E-02-2.505254755564606E-04
 13  8.609198054704826E-14 7.468084497819526E-16
 14  1.473221475300776E-02 1.889084910488786E-04
 15  2.388510605125436E-14 1.290093625153026E-16
 16 -1.180117616299436E-02-1.486138458285876E-04
 17  8.011833099314826E-14 5.398790230366066E-16
 18  9.721161127287606E-03 1.206630867943596E-04
 19  3.266549408682636E-14-2.817295024581096E-17
 20 -8.184674550486538E-03-1.003940281650676E-04
 21  7.645752826513556E-14 4.099372953585576E-16
 22  7.013472031594836E-03 8.517806361922496E-05
 23  3.694856844086046E-14-4.290074449628736E-17
 24 -6.097907448767906E-03-7.343497505593216E-05
 25  6.960090613665686E-14 3.113427325565936E-16
 26  5.367257816926536E-03 6.416540630965666E-05
 27  3.801945712223836E-14-5.374339003347056E-17
 28 -4.774106506811906E-03-5.671057152741196E-05
 29  6.887433071703656E-14 2.601594492666926E-16
 30  4.285626564094736E-03 5.062102932891806E-05
```

```
THE MATRIX OF FOURIER COEF. FOR THE BAFFLE COMP.  1
  1    .68443000763819      7.62391863798555E-04
  2    .26663215104316     -2.33152094424553E-03
  3 -8.82565783269649E-02 -3.00888098471808 4E-04
  4  4.68612639313255E-02  2.99682129160404E-04
  5 -2.98208912488284E-02 -2.30900384944334E-04
  6  2.09347038054192E-02  1.79248849023724E-04
  7 -1.56393908730201E-02 -1.41045424280438E-04
  8  1.22010141941971E-02  1.14417908163099E-04
  9 -9.83215206976046E-03 -9.48846217251626E-05
 10  8.13012918280803E-03  8.02320923332669E-05
 11 -6.87153021073458E-03 -6.90662608458939E-05
 12  5.92633513098945E-03  6.05151277191485E-05
 13 -5.22006094333712E-03 -5.40768933505575E-05
 14  4.72228795561305E-03  4.96181907242946E-05
 15 -4.47718760309154E-03 -4.77978219416034E-05
 16  5.07340708374687E-03  5.56210275253824E-05
 17 -3.19512679211673E-03 -3.41496429522524E-05
 18  2.39547629513930E-03  2.53090282980487E-05
 19 -1.86965691845250E-03 -1.96058817664472E-05
 20  1.48370029882283E-03  1.54738393824547E-05
 21 -1.18566269377634E-03 -1.23135682138742E-05
 22  9.48535843081542E-04  9.81782585020513E-06
 23 -7.56031957418954E-04 -7.80378548546353E-06
 24  5.97429549892687E-04  6.15253425038793E-06
 25 -4.65256587012087E-04 -4.78206561268219E-06
 26  3.54093115956486E-04  3.63343633599405E-06
 27 -2.59889421222492E-04 -2.66295341045534E-06
 28  1.79549378008782E-04  1.83744261754450E-06
 29 -1.10661968356252E-04 -1.13122625327988E-06
 30  5.13209970342602E-05  5.24110538287982E-07

THE MATRIX OF FOURIER COEF. FOR THE BAFFLE COMP.  2
  1  -.68443000763912     -7.62391862154394E-04
  2  -.26663215104372      2.33152094424492E-03
  3  8.82565783270470E-02  3.00888984723000E-04
  4 -4.68612639315571E-02 -2.99682129159580E-04
  5  2.98208912488162E-02  2.30900384946768E-04
  6 -2.09347038055803E-02 -1.78248849023313E-04
  7  1.56393908729862E-02  1.41045424281979E-04
  8 -1.22010141943286E-02 -1.14417908162771E-04
  9  9.83215206971416E-03  9.48846217262798E-05
 10 -8.13012918249207 2E-03 -8.02320923299967E-05
 11  6.87153021066429E-03  6.90662608467374E-05
 12 -5.92633513085559E-03 -6.05151277189345E-05
 13  5.22006094389227E-03  5.40768933512022E-05
 14 -4.72228795569365E-03 -4.96181907241181E-05
 15  4.47718760304763E-03  4.77978219421114E-05
 16 -5.07340708385765E-03 -5.56210275251643E-05
 17  3.19512679201223E-03  3.41496429524552E-05
 18 -2.39547629523654E-03 -2.53090282978554E-05
 19  1.86965651836170E-03  1.96058817666213E-05
 20 -1.48370029890584E-03 -1.54738393822858E-05
 21  1.18566269669947E-03  1.23135682140125E-05
 22 -9.48535843146348E-04 -9.81782585007161E-06
 23  7.56031957362475E-04  7.80378546557840E-06
 24 -5.97429549943938E-04 -6.15253424998734E-06
 25  4.65256586966627E-04  4.78206561270758E-06
 26 -3.54093115993570E-04 -3.63343633592227E-06
 27  2.59889421193649E-04  2.66295341051607E-06
 28 -1.79549378031336E-04 -1.83744261750334E-06
 29  1.10661968341592E-04  1.13122625330407E-06
 30 -5.13209970414586E-05 -5.24110538273396E-07

COMB. INPUT  .411352     NOZZLE EXI.= 5.733113E-03 DISSI.=  .780698

DECAY RATE= 9.93095772017785E-02

DECAY IN DECIBELS /CYCLE=  2.28135728751 01
```

```
      PROGRAM BAFFLE(INPUT,OUTPUT,TAPE5=INPUT,TAPE6=OUTPUT)
      COMPLEX OMEG,AMU,BMU,ANN,ALAMI,CI,Q,ALAMN,CBS,CB1,CB2,ECB1,ECB2,
     1CCC,BSV,BASEV,CCS,BB1,BB2,EB1,EB2,BCC,BASE1,G1,OMEG1,ALINJ,ALNOZ,
     2BASE,SUMX,SUMG,SUMF,BSK,AB1,AB2,CM,BK
      COMPLEX BASEB
      DIMENSION TTI(10,10,12)
      DIMENSION Q(4)
      DIMENSION TTE(10,10,12),BN(10,10),AMC(10,10),BN1(10,10,90)
      DIMENSION W(11),Z(11)
      DIMENSION W1(31),Z1(31)
      COMMON/BLKA/MC,LC,MB,LB,ZB,ALENGTH,AMU(10,10,12),BMU(10,10)
      COMMON/BLKD/DISEV,DISFT,T,GAMMA,TMAX
      COMMON/BLKF/BBES(10,10),CBES(10,10)
      DATA(W(I),I=1,11)/.021291018375S4,.057616658311Z4,.09340039827825,
     1.12052016961432,.13642490095628,.14149370892875,.13642490095628,
     2.12052016961432,.09340039827825,.057616658311Z4,.021291018375S4/
      DATA(Z(I),I=1,11)/.00795731995258,.04691007703067,.12291663671458,
     1.23076534494716,.36018479341911,.50000000000000,.63981520658036,
     2.76923465505284,.87708336328542,.95308992296933,.99204260047427/
      DATA(W1(I),I=1,16)/0.0026887390,0.0075039737,0.0127304237,
     10.0176731804,0.0222948757,0.0267407623,0.0310047839,0.0349276963,
     20.0384248404,0.0415402514,0.0442822215,0.0465632991,0.0483213[illegible]
     30.0495867994,0.0503849228,0.0506650035/
      DATA(Z1(I),I=1,16)/0.0009988507,0.0060037410,0.0161304622,
     10.0313633038,0.0513677338,0.0758967083,0.1047907493,0.1377913[illegible]
     20.1745016294,0.2145139136,0.2574590682,0.3029243265,0.3504099954,
     30.3994029530,0.4494289665,0.5/
      DO 78 I=1,15
      W1(I+16)=W1(16-I)
   78 Z1(I+16)=1.-Z1(16-I)
C**** THE VARIABLE MX DETERMINES IF A STANDING WAVE OR TRAVELING WAVE
C**** SOLUTION IS TO BE USED. MX=0 WILL GIVE THE STANDING WAVE AND MX=
C**** 1 WILL GIVE THE TRAVELING WAVE  ********************************
      MX=1
      MX=0
C**** INPUTS INCLUDE NO. OF FOURIER-BESSEL SERIES TERMS-MC,LC,MB AND LB,
C**** COMBUSTOR LENGTH TO RADIUS-ALENGTH,BAFFLE BLADE LENGTH-ZB,BAFFLE
C**** BLADE THICKNESS-T,NO. OF BAFFLE COMPARTMENTS-MUB,RATIO OF SPECIFIC
C**** HEATS-GAMMA,WAVE AMPLITUDE-EPSILON,MEAN FLOW MACH NO.-AMACH,TRANS-
C**** VERSE MODE CHARACTOR-MHAT,RADIAL MODE CHARACTOR-LHAT,AND MAXIMUM
C**** NO. OF ITERATIONS OF THE SUCCESSIVE APPROX. OF SERIES -IDMAX
      READ(5,200) MC,LC,MB,LB,IDMAX,MHAT,LHAT
  200 FORMAT(7I5)
      READ(5,201) ALENGTH,AMACH,GAMMA,EPSILON
  201 FORMAT(4F10.5)
      READ(5,202) MUB,ZB,T
  202 FORMAT(I5,2F10.5)
      WRITE(6,120)
  120 FORMAT(*1THE FOLLOWING CALCULATIONS ARE PURELY FOR DIAGNOSTIC
     1PURPOSES*,/,* LARGER MATRIX SIZE SHOULD BE USED FOR COMPUTATION*)
      WRITE(6,405)
      WRITE(6,405)
      IF(MX.EQ.0) 407,408
  407 WRITE(6,409)
      GOTO 430
  408 WRITE(6,411)
  430 CONTINUE
      WRITE(6,405)
      WRITE(6,405)
  409 FORMAT(*0THE FOLLOWING CALC.ARE FOR STANDING WAVES*)
  411 FORMAT(*0THE FOLLOWING CALC. ARE FOR TRAVELING WAVES*)
```

```
  405 FORMAT(*0*,75(1H*))
C**** THESE PARAMETERS ARE FOR THE DISSIPATION CALC.
      CTURB=0.05
      VISC=1.E-05
      DISFV=SQRT(VISC)
      DISFT=SQRT(CTURB)
      CALL RCGT(MC,LC,2,CBES)
      CALL RCGT(MB,LB,MUB,BBES)
C**** UNSTEADY COMBUSTION INPUT PARAMETERS N AND TAU ARE DEFINED
      OR=MHAT
      RLMDA=CBES(MHAT+1,LHAT)
      AN=(GAMMA+1.)/4./GAMMA
      TAU=3.14159265359/RLMDA
      WRITE(6,555)
  555 FORMAT(*0THE CYLINDRICAL CHAMBER HAS THE FOLLOWING CONFIG.*)
      WRITE(6,556) ALENGTH,AMACH,GAMMA
  556 FORMAT(*0 THE LENGTH TO RADIUS=*,F10.5,3X,* MEAN FLOW MACH NO.=*,
     1F10.5,3X,/,* RATIO OF SPECIFIC HEATS=*,F10.5)
      WRITE(6,557) LHAT,MHAT,EPSILON
  557 FORMAT(*0THE WAVE CHARACTOR IS *,I3,* RADIAL MODE*,3X,I3,* TRANSV
     1 MODE*,/,* AND IS OF WAVE AMPLITUDE*,G21.14)
      WRITE(6,560) MUB,ZB,T
  560 FORMAT(*0THE BAFFLE CONSISTS OF *,I5,* COMPARTMENTS WITH LENGTH*,
     1F10.5,/,* AND BLADE THICKNESS*,F10.5)
      WRITE(6,559) VISC
  559 FORMAT(*0 MOLECULAR VISCOSITY=*,G21.14)
      WRITE(6,134) CTURB
  134 FORMAT(*0EFFECTIVE TURBULENT VISC. COEF.=*,G21.14)
      PI=3.14159265359
      OR2=MUB
      DO 100 MU=1,MUB
      OR=MU
      V1=2.*3.14159265359*OR/OR2
      V2=2.*3.14159265359*(OR-1.)/OR2
      DO 100 MSTAR=1,MB
      DO 100 M=1,MC
      B1=(MSTAR-1.)*MUB/2.-(M-1.)
      B0=B1*B1
      IF(B0.LT.1.E-06) GOTO 101
      B2=(MSTAR-1.)*MUB/2.+(M-1.)
      BAS1=(SIN(B1*V1)-SIN(B1*V2))/(2.*B1)
      BAS2=(SIN(B2*V1)-SIN(B2*V2))/(2.*B2)
      BAS3=(COS(B1*V1)-COS(B1*V2))/(2.*B1)
      BAS4=(COS(B2*V1)-COS(B2*V2))/(2.*B2)
      IF(M).EQ.0) BAS3=BAS4=0.0
      TTE(MSTAR,M,MU)=BAS1+BAS2
      TTI(MSTAR,M,MU)=BAS3-BAS4
      GOTO 100
  101 EP=1.
      IF(M.EQ.1) EP=2.
      TTE(MSTAR,M,MU)=EP*3.14159265359/MUB
      TTI(MSTAR,M,MU)=0.0
  100 CONTINUE
      EP=1.
      DO 102 M=1,MB
      OR=(M-1.)*MUB/2.
      DO 103 L=1,LB
      B1=BBES(M,L)+1.E-10
      B2=BESSCAL(OR,B1)
      BN(M,L)=PI*EP*B2*B2*(1.-OR*OR/B1/B1)/MUB
  103 CONTINUE
```

```
  102 EP=0.5
      EP=1.
      DO 843 M=1,MC
      OR=M-1.
      DO 155 L=1,LC
      B1=CBES(M,L)+1.E-10
      B2=BESSCAL(OR,B1)
      AMC(M,L)=PI*EP*B2*B2*(1.-OR*OR/B1/B1)
  155 CONTINUE
      IF(MX.EQ.0) EP=0.5
  843 CONTINUE
C**** THE FOLLOWING MATRIX OF INTEGRALS OF PRODUCTS OF BESSEL FUNCTIONS
C**** REPRESENT A MAJOR AMOUNT OF COMPUTING TIME- FOR A PARTICULAR BAFFLE
C**** CONFIGURATION THESE VALUES NEED BE COMPUTED ONLY ONCE AND STORED
      NQ=MC*LC
      DO 156 N=1,NQ
      DO 156 M=1,MB
      DO 156 L=1,LB
  156 BN1(M,L,N)=0.0
      DO 70 M=1,MC
      MG=M-1
      ORC=MG
      DO 72 MP=1,MB
      ORB=(MP-1.)*MUB/2.
      DO 72 L=1,LC
      RLM1=CBES(M,L)
      AL5=BESSCAL(ORC,RLM1/2.)
      NC=L+LC*MG
      DO 72 LP=1,LB
      RLM2=BBES(MP,LP)
      AL6=BESSCAL(ORB,RLM2/2.)
      SUM=0.0
      DO 74 I=1,31
      ALX=Z1(I)
      ALX1=ALX*RLM1*2.
      ALX2=ALX*RLM2*2.
      IF(ORC.GE.5.AND.ALX1.LT.ORC) GOTO 300
      AL3=BESSCAL(ORC,RLM1*ALX)
      GOTO 301
  300 AL3=AL5*((2*ALX)**ORC)
  301 CONTINUE
      IF(ORB.GE.5.AND.ALX2.LT.ORB) GOTO 302
      AL4=BESSCAL(ORB,RLM2*ALX)
      GOTO 303
  302 AL4=AL6*((2.*ALX)**ORB)
  303 CONTINUE
   74 SUM=SUM+ALX*W1(I)*AL3*AL4
      BN1(MP,LP,NC)=SUM
   72 CONTINUE
   70 CONTINUE
      ID=0
      MS=MMAT+1
      NC=LMAT+LC*MMAT
      DO 845 M=1,MC
      DO 845 L=1,LC
  845 AMU(M,L)=CMPLX(0.0,0.0)
      CI=CMPLX(0.0,1.0)
      DO 840 MU=1,MUB
      DO 840 M=1,MM
      DO 840 L=1,LB
  840 AMU(M,L,MU)=(TTE(M,MS,MU)+CI*TTI(M,MS,MU))*BN1(M,L,NC),
```

```
C**** FIRST GUESS OF FREQUENCY
      OMEG=CMPLX(1.0,0.0)
  851 CONTINUE
      NC=LHAT+LC*MHAT
      DEL=0.1
      MS=MHAT+1
      PI=3.14159265359
      Q(1)=CMPLX(0.0,-1.0)
      Q(2)=CMPLX(-1.0,0.0)
      Q(3)=CMPLX(1.0,0.0)
      Q(4)=CMPLX(0.0,1.0)
  222 IN=0
  215 CONTINUE
      ANN=EN*(1.-CEXP(-CI*OMEG*TAU))-1./GAMMA
      ALAMI=-GAMMA*CI*OMEG*AMACH*ANN/(1.+GAMMA*AMACH*AMACH*ANN)
      AB=AMACH*(GAMMA-1.)/2.
      ALAMN=-CI*OMEG*AB/(1.+AMACH*AB)
      CBS=CSQRT(OMEG*OMEG*AMACH*AMACH*(AMACH*AMACH-1.)*(RLMDA*RLMDA-
     1OMEG*OMEG))
      CB1=(OMEG*AMACH+CBS)/(1.-AMACH*AMACH)
      CB2=(OMEG*AMACH-CBS)/(1.-AMACH*AMACH)
      ECB1=CEXP(CI*(CB1-CB2)*(ZB-ALENGTH))
      ECB2=CMPLX(1.0,0.0)
      CCC=-(CI*CB1-ALAMN)/(CI*CB2-ALAMN)
      BSV=CI*(CB1*ECB1+CB2*CCC*ECB2)/(ECB1+CCC*ECB2)
      BASEV=CMPLX(0.0,0.0)
      DO 800 M=1,MB
      CR=(M-1.)*MUA/2.
      DO 800 L=1,LA
      RLMDAB=BBES(M,L)
      CCS=CSQRT(OMEG*OMEG*AMACH*AMACH*(AMACH*AMACH-1.)*(RLMDAB*RLMDAB-
     1OMEG*OMEG))
      BB1=(OMEG*AMACH+CCS)/(1.-AMACH*AMACH)
      BB2=(OMEG*AMACH-CCS)/(1.-AMACH*AMACH)
      EB2=CEXP(CI*(BB2-BB1)*ZB)
      EB1=CMPLX(1.0,0.0)
      BCC=-(CI*BB1-ALAMI)/(CI*BB2-ALAMI)
      BASE1=CMPLX(0.0,0.0)
      DO 881 MU=1,MUB
  881 BASE1=BASE1+AMU(M,L,MU)*(TTE(M,MS ,MU)-CI*TTI(M,MS ,MU))
      BASE1=BASE1*BN1(M,L,NC)
      SUMX=(EB1*EB1+BB2*EB2*BCC)/(EB1+BCC*EB2)
      BASEV=BASEV+BASE1*CI*(BB1*EB1+BB2*EB2*BCC)/(EB1+BCC*EB2)
  800 CONTINUE
      BASEV=BASEV/AMC(MS,LHAT)
      G1=BSV-BASEV
      G=CABS(G1)
      IF(IN.NE.0) GOTO 224
  223 OMEG1=OMEG
      REF=G
      IN=1
      GOTO 225
  224 IF(G.LT.REF) GOTO 223
      IF(IN.LT.4) GOTO 228
      OMEG=OMEG1
      DEL=DEL/2.
      IF(DEL.LT.1.E-04) GOTO 310
      IN=1
      GOTO 225
  228 IN=IN+1
  225 OMEG=OMEG1+Q(IN)*DEL
```

```
      GOTO 215
C**** THIS ITERATED VALUE OF FROUENCY ONLY INCLUDES THE WAVE ALTERATION
C**** EFFECTS OF THE BAFFLE AND CONSEQUENTLY PREDICTS A GROWTH RATE
C**** ENERGY DISSIPATION HASNT BEEN INTRODUCED AT THIS POINT IN THE PROG.
  310 WRITE(6,410) ID,OMEG
  410 FORMAT('0ITERATION',I3,' COMPLEX FREQ.=',2G21.14)
C**** ITERATION OF MAIN CHAMBER COEFS.
      ALINJ=ALAMI
      ALNOZ=ALAMN
      DO 809 MST=1,MC
      MSQ=MST-1
      ORI=MST-1.
      DO 811 LST=1,LC
      IF(MST.EQ.MS.AND.LST.EQ.LHAT) GOTO 811
      NCI=LST+LC*(MST-1.)
      RLMDA1=CBES(MST,LST)
      BASE=OMEG*OMEG*AMACH*AMACH+(AMACH*AMACH-1.)*(   RLMDA1*RLMDA1-
     1OMEG*OMEG)
      BASE=CSQRT(BASE)
      CB1=(OMEG*AMACH+BASE)/(1.-AMACH*AMACH)
      CB2=(OMEG*AMACH-BASE)/(1.-AMACH*AMACH)
      CCC=-(CI*CB1-ALNOZ)/(CI*CB2-ALNOZ)
      ECB1=CEXP(CI*(CB1-CB2)*(ZB-ALENGTH))
      ECB2=CMPLX(1.0,0.0)
      CBS=CI*(CB1*ECB1+CB2*CCC*ECB2)/(ECB1+CCC*ECB2)
      BASEG=AMC(MST,LST)
      SUMX=CMPLX(0.0,0.0)
      DO 814 M=1,MB
      OR=(M-1.)*MUB/2.
      DO 814 L=1,LB
      RLM=BBES(M,L)
      CCS=CSQRT(OMEG*OMEG*AMACH*AMACH+(AMACH*AMACH-1.)*(RLM*RLM-
     1OMEG*OMEG))
      BB1=(OMEG*AMACH+CCS)/(1.-AMACH*AMACH)
      BB2=(OMEG*AMACH-CCS)/(1.-AMACH*AMACH)
      EB1=CMPLX(1.0,0.0)
      EB2=CEXP(CI*(BB2-BB1)*ZB)
      BCC=-(CI*BB1-ALINJ)/(CI*BB2-ALINJ)
      BASE=CI*(BB1*EB1+BB2*EB2*BCC)/(EB1+BCC*EB2)
      SUMG=CMPLX(0.0,0.0)
      DO 817 MU=1,MUB
  817 SUMG=SUMG+AMU(M,L,MU)*(TTE(M,MST,MU)-CI*TTI(M,MST,MU))
      SUMG=SUMG*BN1(M,L,NC1)
  814 SUMX=SUMX+SUMG*BASE
      BMU(MST,LST)=SUMX/BASEG/CBS
  811 CONTINUE
  809 CONTINUE
      BMU(MS,LHAT)=CMPLX(1.0,0.0)
      ID=ID+1
      DO 960 M=1,MB
      OR=(M-1.)*MUB/2.
      DO 960 L=1,LB
      DO 970 MU=1,MUB
      SUMF=CMPLX(0.0,0.0)
      DO 971 MP=1,MC
      DO 971 LP=1,LC
      NC=LP+LC*(MP-1.)
      SUMF=SUMF+BMU(MP,LP)*BN1(M,L,NC)*(TTE(M,MP,MU)+CI*TTI(M,MP,MU))
  971 CONTINUE
  970 AMU(M,L,MU)=SUMF/BN(M,L)
  960 CONTINUE
```

```
      IF(IC.LT.IOMAX) GOTO 851
      WRITE(6,909)
  909 FORMAT('0THE FOURIER-BESSEL COEFS. FOR MAIN CHAMBER')
      DO 911 M=1,MC
      WRITE(6,910) M,(BMU(M,L),L=1,LC)
  911 CONTINUE
  910 FORMAT(' ',I3,' ',10G10.3,/,10G10.3)
      DO 912 IO=1,MUB
      WRITE(6,913)IO
  913 FORMAT('0THE FOURIER-BESSEL COEFS. FOR BAFFLE COMPARTMENT',I3)
      DO 914 M=1,MB
      WRITE(6,910) M,(AMU(M,L,IO),L=1,LB)
  914 CONTINUE
  912 CONTINUE
C**** STABILITY CALC.
      OMG=REAL(OMEG)
      BINI=0.0
      SUMY1=0.0
      DO 821 M=1,MB
      OR=(M-1.)*MUB/2.
      DO 821 L=1,LB
      RLM=BBES(M,L)
      BSK=CSQRT(OMEG*OMEG*AMACH*AMACH*(AMACH*AMACH-1.)*(RLM*RLM-
     1OMEG*OMEG))
      AB1=(OMEG*AMACH+BSK)/(1.-AMACH*AMACH)
      AB2=(OMEG*AMACH-BSK)/(1.-AMACH*AMACH)
      CM=-(CI*AB1-ALINJ)/(CI*AB2-ALINJ)
      BASE=CEXP(CI*AB1*ZB)+CM*CEXP(CI*AB2*ZB)
      BAS=CABS(BASE)
      BAS=BAS*BAS
      BB1=(1.+CM)*CI*OMEG-AMACH*CI*(AB1+AB2*CM)
      BASR=CABS(BB1)
      BASR=BASR*BASR*GAMMA*GAMMA
      SUMW1=0.0
      DO 822 I=1,11
      ETA=ZB*Z(I)
      BSK=CEXP(CI*AB1*ETA)+CM*CEXP(CI*AB2*ETA)
      BS1=CABS(BSK)
      BB2=CI*(AB1*CEXP(CI*AB1*ETA)+CM*AB2*CEXP(CI*AB2*ETA)
      BSK=GAMMA*(CI*OMEG*BSK+AMACH*BB2)
      BS =CABS(BSK)
      BS=BS*BS/2./GAMMA+GAMMA*OMG*OMG*BS1*BS1/2.
  822 SUMW1=SUMW1+BS*W(I)*ZB/BAS
      RAM=0.0
      DO 823 MU=1,MUB
      RAM1=CABS(AMU(M,L,MU))
  823 RAM=RAM+RAM1*RAM1
      BINI=BINI+RAM*BASR*BN(M,L)/BAS
  821 SUMY1=SUMY1+RAM*SUMW1*BN(M,L)
      BNZI=0.0
      SUMU1=0.0
      DO 841 M=1,MC
      OR=M-1.
      DO 841 L=1,LC
      RLM=CBES(M,L)
      BK=CSQRT(OMEG*OMEG*AMACH*AMACH*(AMACH*AMACH-1.)*(RLM*RLM-
     1OMEG*OMEG))
      CB1=(OMEG*AMACH+BK)/(1.-AMACH*AMACH)
      CB2=(OMEG*AMACH-BK)/(1.-AMACH*AMACH)
      CM=-(CI*CB1-ALAMN)/(CI*CB2-ALAMN)
      BASE=CEXP(CI*(CB1-CB2)*(ZB-ALENGTH))*CM
```

```
      BAS=CABS(BASE)
      BAS=BAS*BAS
      BASEB=CEXP(-CI*CB2*(ZB-ALENGTH))
      BBS=CABS(BASEB)
      BBS=BBS*BBS
      BB1=(1.+CM)*CI*OMEG*AMACH*CI*(CB1+CM*CB2)
      BASR=CABS(BB1)
      BASR=BASR*BASR*GAMMA*GAMMA
      SUMV1=0.0
      DO 842 I=1,11
      ETA=ZB+(ALENGTH-ZB)*Z(I)
      BSK=CEXP(CI*(CB1-CB2)*(ETA-ALENGTH))+CM
      BS1=CABS(BSK)
      BB2=CI*(CM1*CEXP(CI*(CB1-CB2)*(ETA-ALENGTH))+CM*CB2)
      BSK=GAMMA*(CI*OMEG*BSK+AMACH*BB2)
      BS =CABS(BSK)
      BS=BS*BS/2./GAMMA+GAMMA*OMG*OMG*BS1*BS1/2.
      BASEB=CEXP(-CI*CB2*(ZB-ETA))
      BCS=CABS(BASEB)
      BCS=BCS*BCS
  842 SUMV1=SUMV1+BCS*BS*W(I)*(ALENGTH-ZB)/BAS
      RAM1=CABS(BMU(M,L))
      BNZI=BNZI+RAM1*RAM1*BASR*AMC(M,L)*BBS/BAS
  841 SUMU1=SUMU1+RAM1*RAM1*AMC(M,L)*SUMV1
      T=T/2.
      CALL VDISP(OMG,MUB,EPSILON,AMACH,SUM)
      BINIR=EINI/2.
      BNZIR=ENZI/2.
      FN=AN*(1.-COS(OMG*TAU))*AMACH
      ANZB=AMACH*(1.+GAMMA)/2./GAMMA
      BINIR=FN*BINIR
      BNZIR=ANZB*BNZIR
      SUMIN=BNZIR-BINIR*SUM
      WRITE(6,30) BINIR,BNZIR,SUM
   30 FORMAT(*0COMB. INPUT*,G13.6,* NOZZLE EXT.=*,G13.6,* DISSI.=*,G13.6
     1)
      SUMY1=SUMU1+SUMY1
C**** DECAY RATE CALC.
      DECYRT=SUMIN/SUMY1
      WRITE(6,125) DECYRT
  125 FORMAT(*0DECAY RATE=*,G21.14)
      DECTB=54.575*DECYRT/OMEG
      WRITE(6,130) DECTB
  130 FORMAT(*0DECAY IN DECIBELS/CYCLE=*,G21.14
      END
```

```
      SUBROUTINE VDISP(OMEG,MUB,EPSILON,AMACH,VALUE)
      COMPLEX A,AMU,BMU,SUM,SUMX
      DIMENSION A(12,11)
      DIMENSION W(11),Z(11)
      COMMON/BLKA/MC,LC,MB,LB,ZB,ALENGTH,AMU(10,10,12),BMU(10,10)
      COMMON/BLKD/DISFV,DISFT,T,GAMMA,TMAX
      COMMON/BLKF/BBES(10,10),CBES(10,10)
      DATA(W(I),I=1,11)/.02129101837554,.05761665831124,.09340039827825,
     1.12052016961432,.13642490095628,.14149370892875,.13642490095628,
     2.12052016961432,.09340039827825,.05761665831124,.02129101837554/
      DATA(Z(I),I=1,11)/.00795731995258,.04691007703067,.12291663671458,
     1.23076534494716,.36018479341911,.50000000000000,.63981520658089,
     2.76923465505284,.87708336328542,.95308992296933,.99204268004742/
C**** DISSIPATION CALCULATION IS AS FOLLOWS
      PI=3.14159265359
C**** SMALLEST VALUE FOR RADMIN=MUB*T/PI
      RADMIN=MUB*T/PI
      DO 331 I=1,11
      R=RADMIN+(1.-RADMIN)*Z(I)
      TMAX=T/R
      DO 331 MU=1,MUB
      THETAX=2.*PI*MU/FLOAT(MUB)+TMAX
      THETA =2.*PI*MU/FLOAT(MUB)-TMAX
      TH=2.*PI*MU/FLOAT(MUB)
      AL=MB*LB
      SUMX=CMPLX(0.0,0.0)
      SUM=CMPLX(0.0,0.0)
      DO 332 M=1,MB
      OR=(M-1.)*MUB/2.
      DO 332 L=1,LB
      V=BBES(M,L)
      V2=BESSCAL(OR,V/2.)
      V=V*R
      V3=V*2.
      IF(OR.GE.5.AND.V3.LT.OR) GOTO 300
      V1=BESSCAL(OR,V)
      GOTO 301
  300 V1=V2*((R*2.)**OR)
  301 CONTINUE
      MUX=MU+1
      IF(MU.EQ.MUB) MUX=1
      SUMX=SUMX+AMU(M,L,MUX)*V1*COS(OR*THETAX)
  332 SUM=SUM+AMU(M,L,MU)*V1*COS(OR*THETA)
      A(MU,I)=(SUMX-SUM)/SQRT(2.*T)
  331 CONTINUE
      AMULT=GAMMA*SQRT(OMEG/2.)/2.
      SUM=CMPLX(0.0,0.0)
      DO 339 J=1,11
      TE=ACOS(ZB/(ZB+T))
      DO 339 MU=1,MUB
      AX=CABS(A(MU,J))
      AX=AX*AX
      B=EPSILON*EPSILON*AX/T/4.
      SUMI=0.0
      DO 336 I=1,11
      ETA=TE/2.+Z(I)*(PI-TE)/2.
      V1=SIN(ETA)
  336 SUMI=SUMI+(DISFV+DISFT*((AMACH*AMACH+B*V1*V1)**0.25))*W(I)/V1
      SUMI=SUMI*AX*(PI-TE)/2.
  339 SUM=SUM+SUMI*W(J)*(1.-RADMIN)
      VALUE=AMULT*SUM
      RETURN
      END
```

```
      FUNCTION BESSCAL(OR,ALX)
C**** THIS SUBPROGRAM CALCULATES THE VALUE OF THE BESSEL FUNCTION OF
C**** INTEGER AND HALF INTEGER ORDER-OR WITH ARGUMENT -ALX
      M=OR
      A3=(OR-M)*(OR-M)
      IF(A3.GT.0.001) GOTO 100
      IF(ALX.GE.3.0) GOTO 101
      AL2=ALX*ALX/3./3.
      AL4=AL2*AL2
      AL6=AL2*AL4
      AL8=AL4*AL4
      AL10=AL8*AL2
      AL12=AL6*AL6
      BASE1=1.0-2.2499997*AL2+1.2656208*AL4-0.3163866*AL6+0.0444479*AL8-
     10.0039444*AL10+0.0002100*AL12
      BASE2=0.5-0.56249985*AL2+0.21093573*AL4-0.03954289*AL6+0.00443319*
     1AL8-0.00031761*AL10+0.00001109*AL12
      BASE2=ALX*BASE2
      GOTO 200
  101 AL1=3./ALX
      AL2=AL1*AL1
      AL3=AL2*AL1
      AL4=AL2*AL2
      AL5=AL3*AL2
      AL6=AL3*AL3
      F1=0.79788456-0.00000077*AL1-0.0055274*AL2-0.00009512*AL3+
     10.00137237*AL4-0.00072805*AL5+0.00014476*AL6
      THETA1=ALX-0.78539816-0.04166397*AL1-0.00003954*AL2+0.00262573*
     1AL3-0.00054125*AL4-0.00029333*AL5+0.00013558*AL6
      F2=0.79788456+0.00000156*AL1+0.01659667*AL2+0.00017105*AL3-
     10.00249511*AL4+0.00113653*AL5-0.00020033*AL6
      THETA2=ALX-2.35619449+0.12499612*AL1+0.00005650*AL2-0.00637879*AL3
     1+0.00074348*AL4+0.00079824*AL5-0.00029166*AL6
      B1=ALX**0.5
      BASE1=F1*COS(THETA1)/B1
      BASE2=F2*COS(THETA2)/B1
  200 IF(M.EQ.0) GOTO 201
      IF(M.EQ.1) 202,203
  201 BESSCAL=BASE1
      RETURN
  202 BESSCAL=BASE2
      RETURN
  203 CONTINUE
      M1=M-1
      DO 204 M2=1,M1
      BASE3=2.*M2*BASE2/ALX-BASE1
      BASE1=BASE2
      BASE2=BASE3
  204 CONTINUE
      BESSCAL=BASE2
      RETURN
  100 CONTINUE
      BASE=(2.0/3.1415926/ALX)**0.5
      BASE1=COS(ALX)*BASE
      BASE2=SIN(ALX)*BASE
      IF(M.EQ.0) 220,223
  220 BESSCAL=BASE2
      RETURN
  223 M1=M
      DO 224 M2=1,M1
      AM3=M2-0.5
```

```
      BASE3=2.*AM3*BASE2/ALX-BASE1
      BASE1=BASE2
      BASE2=BASE3
  224 CONTINUE
      BESSCAL=BASE2
      RETURN
      END
```

```
      SUBROUTINE ROOT(MX,LX,MUB,R
      DIMENSION RT(10,10)
      DO 120 M=1,MX
      OR=MUB*(M-1.)/2.
      OR3=OR**0.33333
      RT(M,1)=0.0
      IF(M.EQ.1) GOTO 140
      RT(M,1)=OR+0.8086165*OR3+0.07249/OR3-0.05097/OR+0.0094*OR3/OR**2
  140 CONTINUE
      DO 121 L=2,LX
      Z=RT(M,L-1)+3.1415926535
      DIR=1
      DEL=0.1
      REF=OR*BESSCAL(OR,Z)/Z-BESSCAL(OR+1,Z)
  100 Z=Z+DEL*DIR
      REF1=OR*BESSCAL(OR,Z)/Z-BESSCAL(OR+1,Z)
      V=REF1/REF
      IF(V.GT.0) GOTO 100
      IF(DEL.LT.1.0E-04) GOTO 105
      DEL=DEL/2.
      DIR=-DIR
      REF=REF1
      GOTO 100
  105 RT(M,L)=Z
  121 CONTINUE
  120 CONTINUE
      RETURN
      END
```

```
THE FOLLOWING CALCULATIONS ARE PURELY FOR DIAGNOSTIC      PURPOSES
LARGER MATRIX SIZE SHOULD BE USED FOR COMPUTATION

**********%**********%**********%**********%**********%**********%**********

**********%**********%**********%**********%**********%**********%**********

THE FOLLOWING CALC.ARE FOR STANDING WAVES

**********%**********%**********%**********%**********%**********%**********

**********%**********%**********%**********%**********%**********%**********

THE CYLINDRICAL CHAMBER HAS THE FOLLOWING CONFIG.

 THE LENGTH TO RADIUS=    1.50000     MEAN FLOW MACH NO.=      .10000
RATIO OF SPECIFIC HEATS=    1.20000

THE WAVE CHARACTOR IS    1 RADIAL MODE      1 TRANSV  MODE
AND IS OF WAVE AMPLITUDE  .10000000000000

THE BAFFLE CONSISTS OF      3 COMPARTMENTS WITH LENGTH      .50000
AND BLADE THICKNESS     .10000

 MOLECULAR VISCOSITY= 1.00000000000000E-05

EFFECTIVE TURBULENT VISC. COEF.= 5.00000000000000E-02

ITERATION  0 COMPLEX FREQ.=  1.666406249999     -3.613281249999996E-02

ITERATION  1 COMPLEX FREQ.=  1.5890624999999    -5.253906249999991E-02

ITERATION  2 COMPLEX FREQ.=  1.6240234374999    -3.964843749999988E-02

ITERATION  3 COMPLEX FREQ.=  1.6082031249999    -4.863281249999982E-02

ITERATION  4 COMPLEX FREQ.=  1.6154296874999    -4.277343749999980E-02

THE FOURIER-BESSEL COEFS. FOR MAIN CHAMBER
  1 -4.066E-16 1.052E-15 2.024E-14 1.093E-14
  2   1.00      0.          .133     1.017E-02
  3  -.245     -3.494E-02-9.036E-02-2.309E-03
  4 -2.233E-13-7.329E-14-5.905E-14-4.997E-15
  5   .121      7.641E-03 5.256E-02-1.791E-03

THE FOURIER-BESSEL COEFS. FOR BAFFLE COMPARTMENT  1
  1   .222      2.955E-03-9.514E-02 5.427E-04
  2   .540     -3.071E-02  .109     8.315E-03
  3  -.200     -1.045E-02-8.382E-02-4.659E-03
  4   .209      1.123E-02 9.777E-02 6.530E-04
  5 -8.901E-02-4.356E-03-4.616E-02-1.086E-03

THE FOURIER-BESSEL COEFS. FOR BAFFLE COMPARTMENT  2
  1  -.443     -5.911E-03  .190    -1.085E-03
  2 -1.814E-13 4.838E-15-3.641E-14-1.521E-15
  3   .400      2.091E-02  .168     9.319E-03
  4 -2.761E-13 8.218E-15-1.151E-13 9.525E-16
  5   .178      8.712E-03 9.232E-02 2.172E-03

THE FOURIER-BESSEL COEFS. FOR BAFFLE COMPARTMENT  3
  1   .222      2.955E-03-9.514E-02 5.427E-04
  2  -.540      3.071E-02 -.109    -8.315E-03
  3  -.200     -1.045E-02-8.382E-02-4.659E-03
  4  -.209     -1.123E-02-9.777E-02-6.530E-04
  5 -8.901E-02-4.356E-03-4.616E-02-1.086E-03

COMB. INPUT  .108318     NOZZLE EXT.= 3.177977E-02 DISSI.=  .418200

DECAY RATE=  .20905835299386

DECAY IN DECIBELS/CYCLE=  7.0577917121102
```